vsparticle

Materials

Input

- Metals
- Alloys
- Metal oxides
- Semiconductors

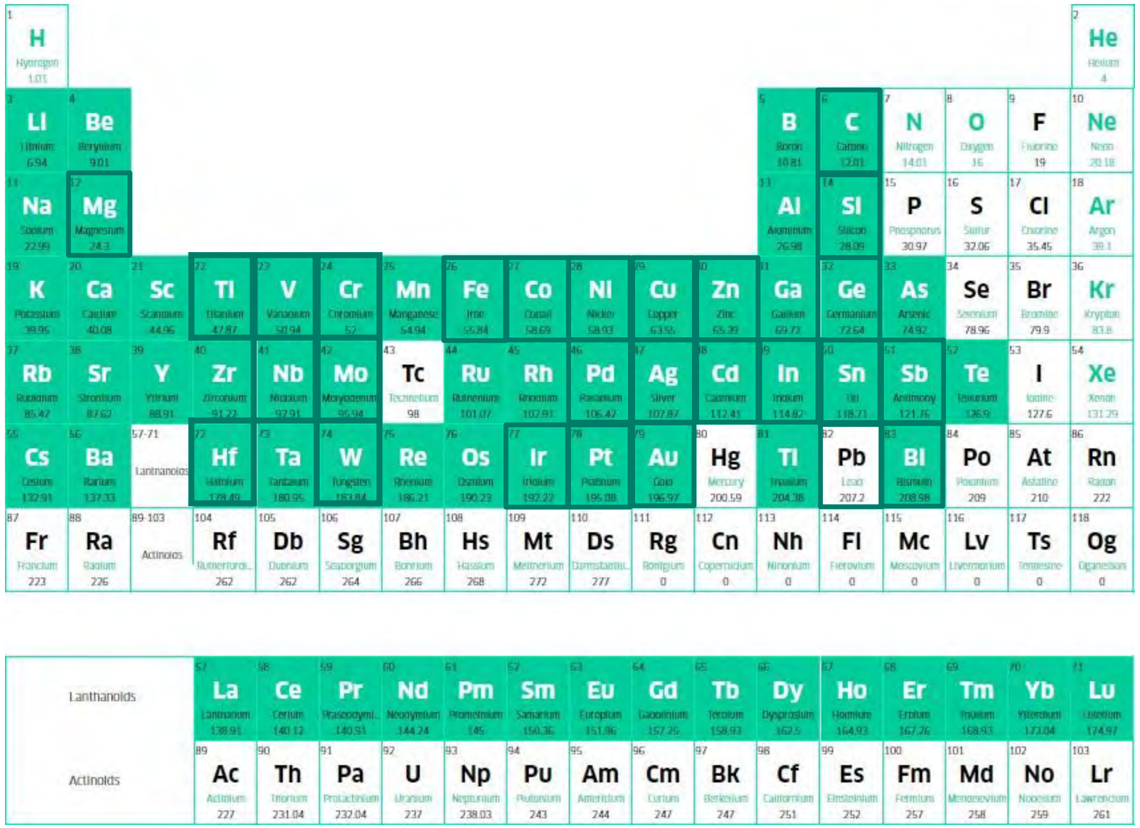

Research interest

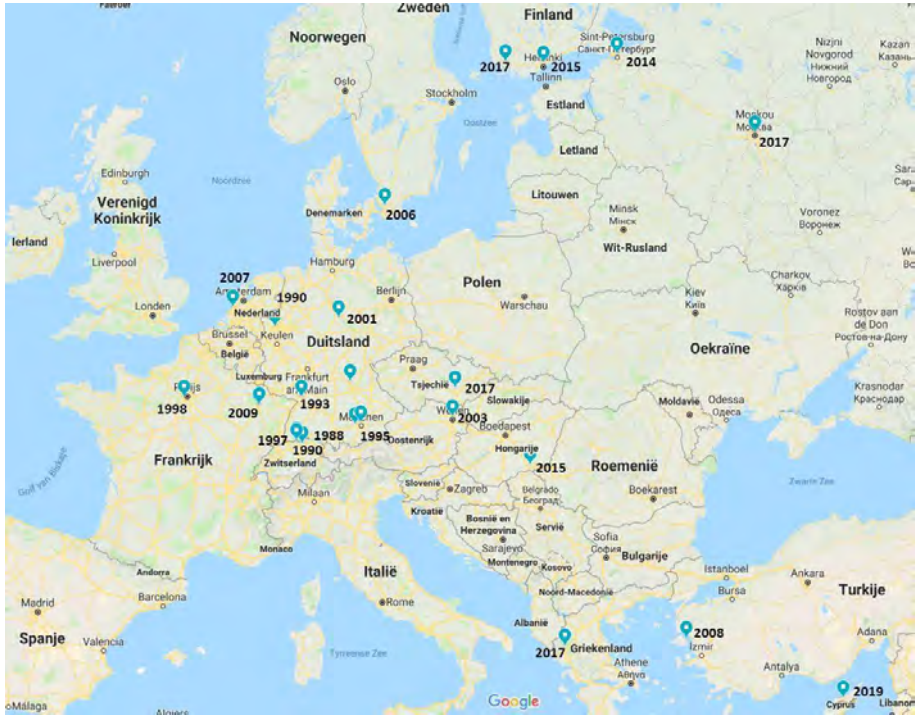

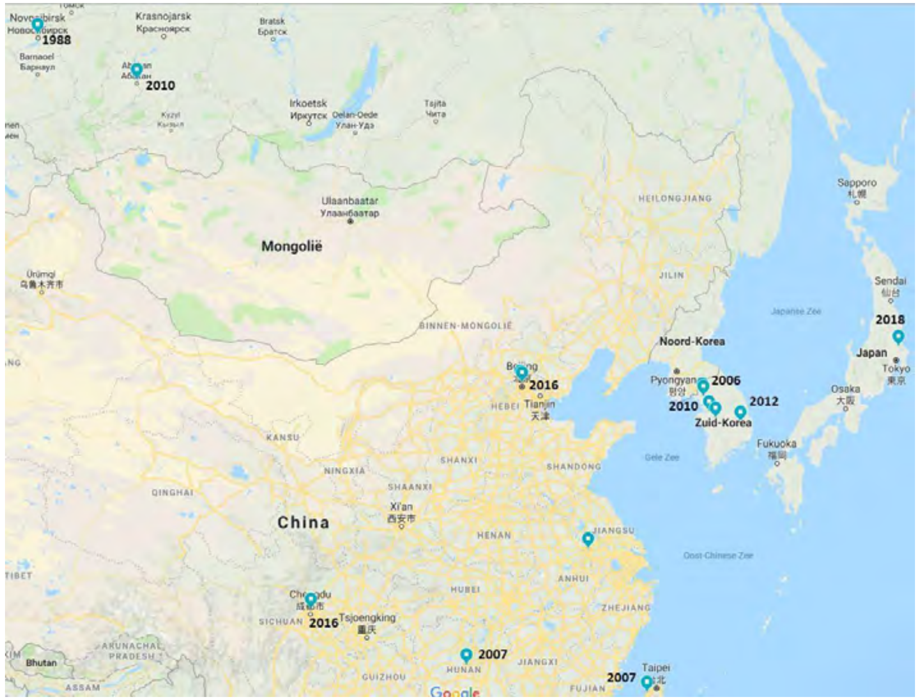

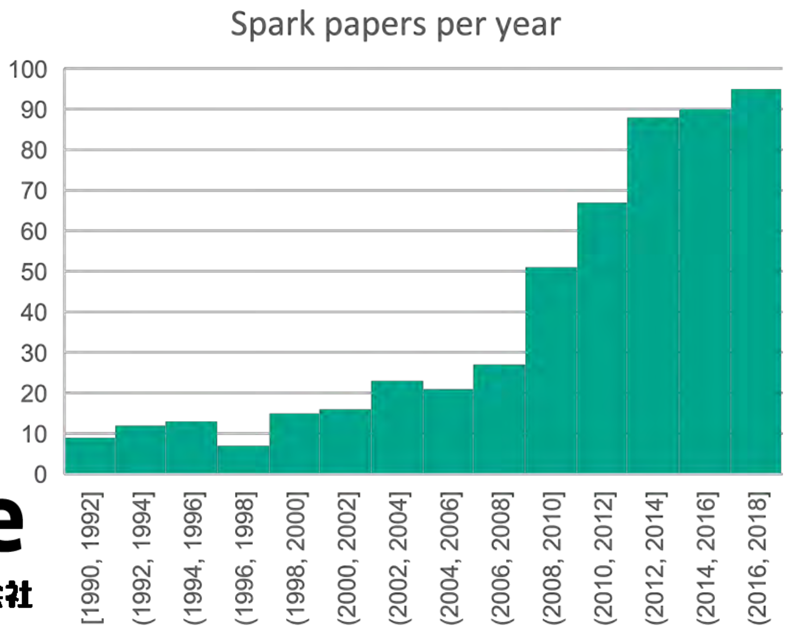

vsparticle

Dylec 東京ダイレック株式会社

Developments

Technical

Proof of principle

1982

- 3-16 nm C and Ag particles

VOLUME 48, NUMBER 25 PHYSICAL REVIEW LETTERS 21 JUNE 1982

Enormous Enhancement of van der Waals Forces between Small Silver Particles

Heinz Burtscher
Laboratory for Solid State Physics, Eidgenossische Technische Hochschule, CH-8093 Zürich, Switzerland

and

Andreas Schmidt-Ott
Atmospheric Physics and Laboratory for Solid State Physics, Eidgenossische Technische Hochschule, CH-8093 Zürich, Switzerland

(Received 4 December 1981)

Dispersion forces enhance the coagulation rate of small particles in a gas. Measurements of coagulation rates on ultrafine Ag and C particles with radii of 3–16 nm were performed. The results obtained with C particles almost agree with the expectations based on bulk electronic properties. However, Ag particles 14 nm in radius exhibit a very large coagulation rate. It points to an enhancement of the dispersion forces of at least a factor of 10^4.

Heinz Burtscher and Andreas Schmidt-Ott. Enormous enhancement of van der waals forces between small silver particles. *Phys. Rev. Lett.*, 48:1734–1737, Jun 1982.

Developments

Technical

First prototype

1988

- Spark under N_2 atmosphere
- Ambient pressure
- Measurement of charged gold particles

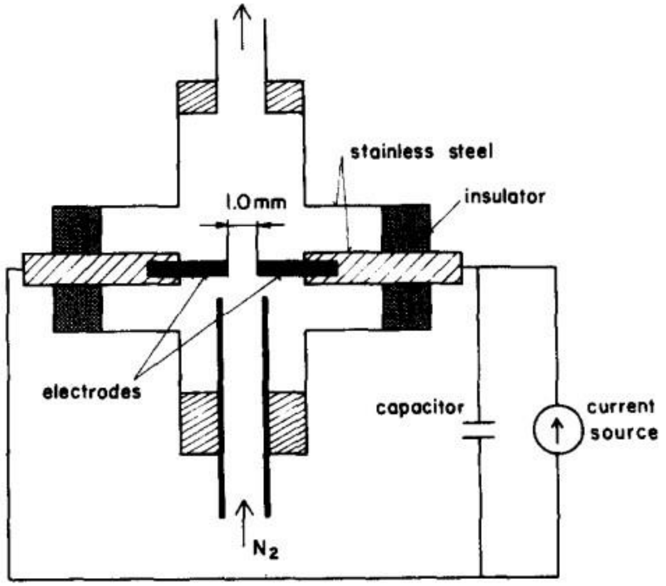

Fig. 1. Schematic of the generator.

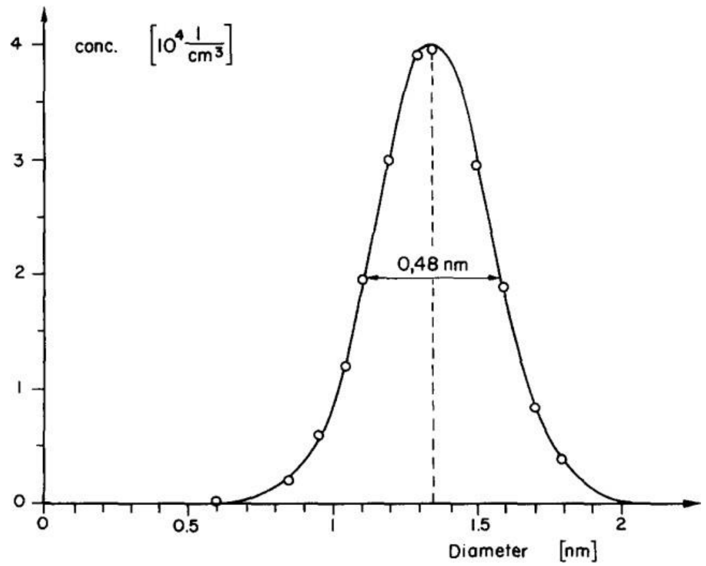

Fig. 5. Size distribution of primary gold particles.

S Schwyn, E Garwin, and A Schmidt-Ott. Aerosol generation by spark discharge. *Journal of Aerosol Science*, 19(5):639 – 642, 1988.

Developments

Output

Monodisperse output

1991

- Deposition of charged silver particles
- Size selection based on electrical mobility
- 8 nm deposited on carbon film

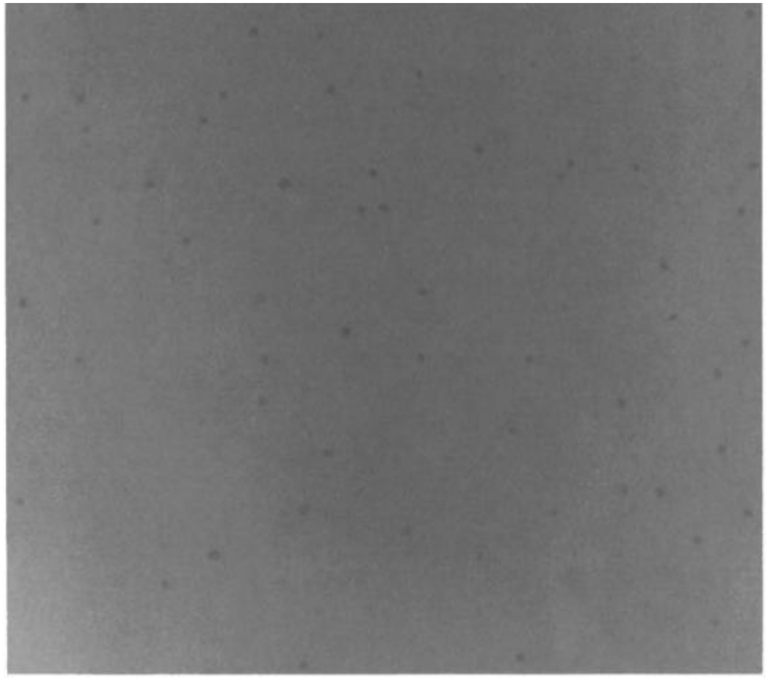

Fig. 1. TEM image of a carbon thin film covered with Ag particles. The particle diameter is 8 nm. The particle concentration is 120 particles per μm^2 after a sampling time of 2 h

B. Schleicher, Th. Jung, H. Hug, and H. Burtscher. Ultrafine particles adsorbed on hopg measured by stm. *Zeitschrift für Physik D Atoms, Molecules and Clusters*, 19(4):327–331, Mar 1991.

Developments

Clusters

Output

1991

- Atomic clusters 1 – 40 Pd, Al atoms
- Setup in vacuum

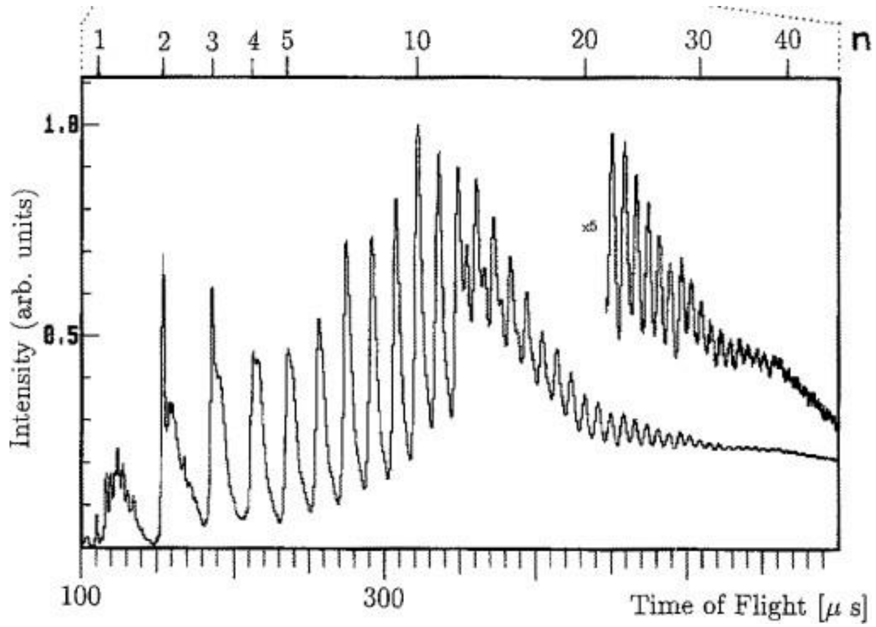

H. R. Siekmann, Ch. Lüder, J. Faehrmann, H. O. Lutz, and K. H. Meiwes-Broer. The pulsed arc cluster ion source (pacis). *Zeitschrift für Physik D Atoms, Molecules and Clusters*, 20(1):417–420, Mar 1991.

Developments

Output

Narrow size distribution for large particles

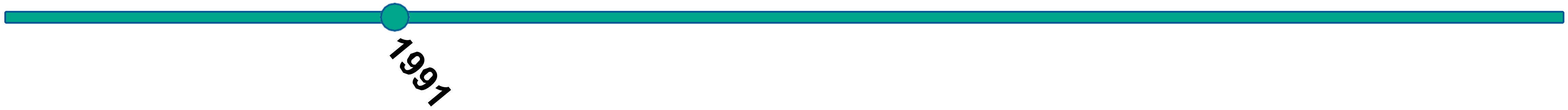

- Particle size distribution has a fixed width (1.27 < σ < 1.34)
- For large particles, the absolute spread is larger
- By continuously adding small NPs to the aerosol, the absolute width can remain constant (1 nm)

Themis Matsoukas and Erdogan Gulari. Self-sharpening distributions revisited—polydispersity in growth by monomer addition. *Journal of Colloid and Interface Science*, 145(2):557 – 562, 1991.

Developments

Technical

First commercial spark generator

1993

- Production of carbon nanoparticles
- 8 mg/h output
- Relatively large particles

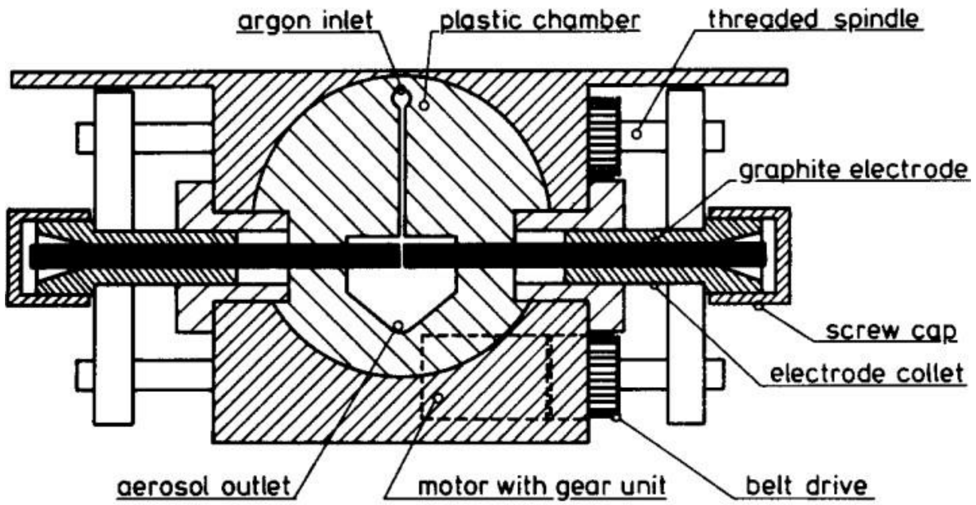

Fig. 1. Mechanical arrangement of the carbon aerosol generator.

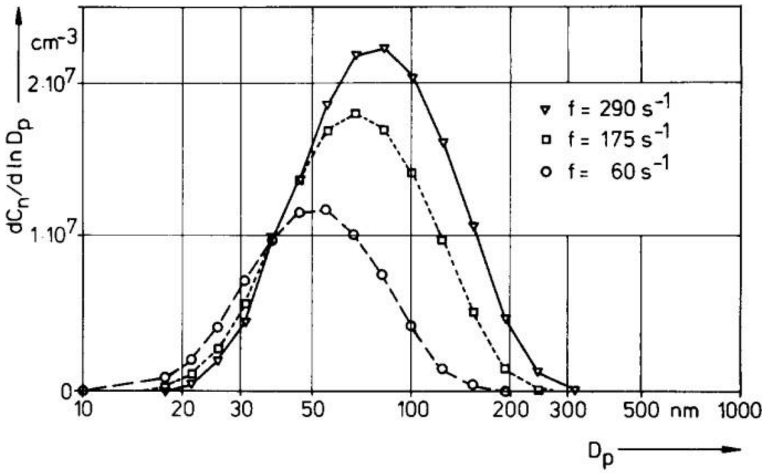

Fig. 5. Particle number distribution of the carbon aerosol for different spark repetition frequencies. Argon flow rate: 6.5 ℓ min^{-1}, dilution air flow rate: 21.0 ℓ min^{-1}.

C. Helsper, W. Mölter, F. Löffler, C. Wadenpohl, S. Kaufmann, and G. Wenninger. Investigations of a new aerosol generator for the production of carbon aggregate particles. *Atmospheric Environment. Part A. General Topics*, 27(8):1271 – 1275, 1993.

Developments

Application

Aerosol catalysis

1999

- Methanation: $4\ H_2 + CO_2 \rightarrow CH_4 + 2\ H_2O$ using Ni

Table 1. Properties of the Ni aerosol catalyst before and after heating for 7 s at 450°C

Sampling location	Specific surface area (m^2/g)	Aerosol mass conc. (μg/cc)	Surf. conc. (BET) (cm^2/cc)	Surf. conc. (SMPS) (cm^2/cc)	Geom. mean diameter (nm)	Primary particle diam. (nm)
Before heating section	173.6	0.0799	0.1387	0.0650	144	3.9
Behind heating section	165.5	0.0465	0.0796	0.0429	103	4.1

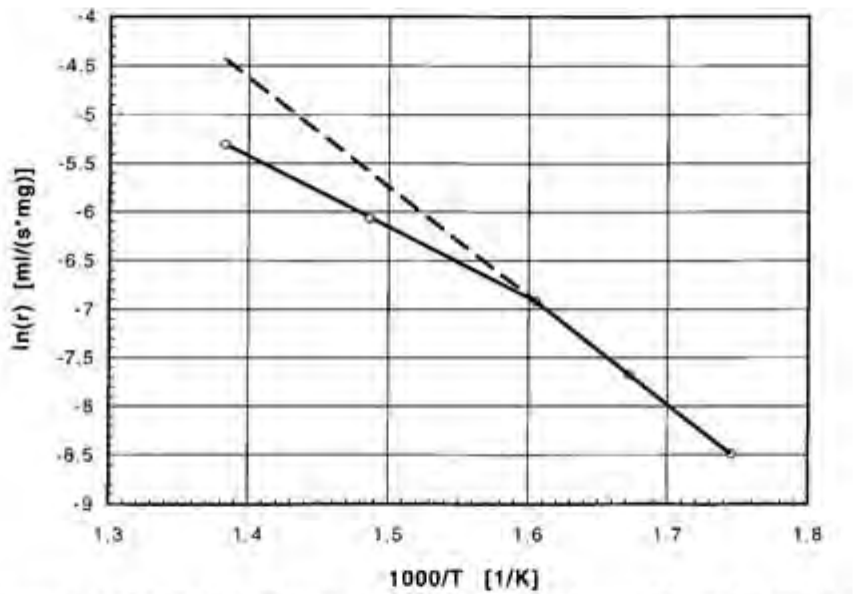

Figure 7. Arrhenius plot of the reaction rate for methanation on airborne Ni particles.

Alfred P. Weber, Martin Seipenbusch, Christoph Thanner, and Gerhard Kasper. Aerosol catalysis on nickel nanoparticles. *Journal of Nanoparticle Research*, 1(2):253–265, Jun 1999.

Developments

Application

Radiolabeling of carbon aerosol

2000

- Application of radioactive Tc in liquid applied to spark electrodes

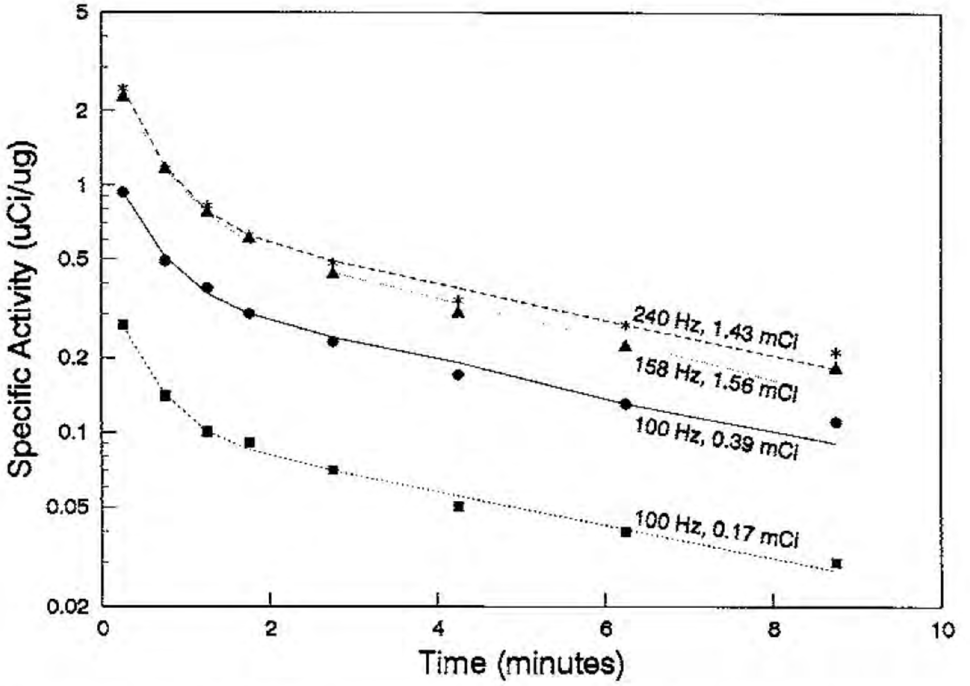

FIGURE 5. Specific activity of aerosol decreases as the sum of a fast and a slow exponential decay function of generator operation time. The half times for fast and slow generator output phases were 0.4 min and 4.8 min, respectively. Notations on curves are the electrode arcing frequency and activity applied to the electrodes.

James S. Brown, Chong S. Kim, Parker C. Reist, Kirby L. Zeman, and William D. Bennett. Generation of radiolabeled "soot-like" ultrafine aerosols suitable for use in human inhalation studies. *Aerosol Science and Technology*, 32(4):325–337, 2000.

Developments

Synthesis of oxides

Material

2004

Table 1

Characteristics of ultrafine aerosols generated for various operation parameters of the generator

	Operation conditions				Particle characteristics			Mass-related surface area		Volume-related surface area	
Particle material	Discharge frequency (Hz)	Argon flow rate (lpm)	Nitrogen flow rate (lpm)	Air flow rate (lpm)	Modal diameter (nm)	Number concentration (cm^{-3})	Mass concentration ($\mu g\ m^{-3}$)	BET_m ($m^2\ g^{-1}$)	ASA_m ($m^2\ g^{-1}$)	BET_v ($m^2\ cm^{-3}$)	ASA_v ($m^2\ cm^{-3}$)
Carbon	3	6.3	17	170	25	10^6	25	750	47	1425	90
Carbon	300	6.3	17	125	70	10^7	115	750	17	1425	32
Carbon	300	6.3	0	125	150	n.a.	n.a.	n.a.	n.a.	n.a.	n.a.
Silver	300	3.5	0	125	20	3×10^6	133	20	11	210	115
Iridium	140	6.3	0	125	18	2.5×10^6	83	n.a.	n.a.	n.a.	n.a.
Iridium	500	6.3	0	125	22	3×10^7	480	123	5.1	2766	102
Ferric oxide	20	5.4	17	165	35	10^6	40	300	10	1560	57
Cadmium oxide	6	3.5	17	165	35	10^6	65	50	9.2	408	75
Cadmium oxide	300	3.5	17	125	50	8×10^6	420	n.a.	n.a.	n.a.	n.a.

C. Roth, G. A. Ferron, E. Karg, B. Lentner, G. Schumann, S. Takenaka, and J. Heyder. Generation of ultrafine particles by spark discharging. *Aerosol Science and Technology*, 38(3):228–235, 2004.

vsparticle

Dylec 東京ダイレック株式会社

Developments

Material

Synthesis of titania by sparking in air

2007

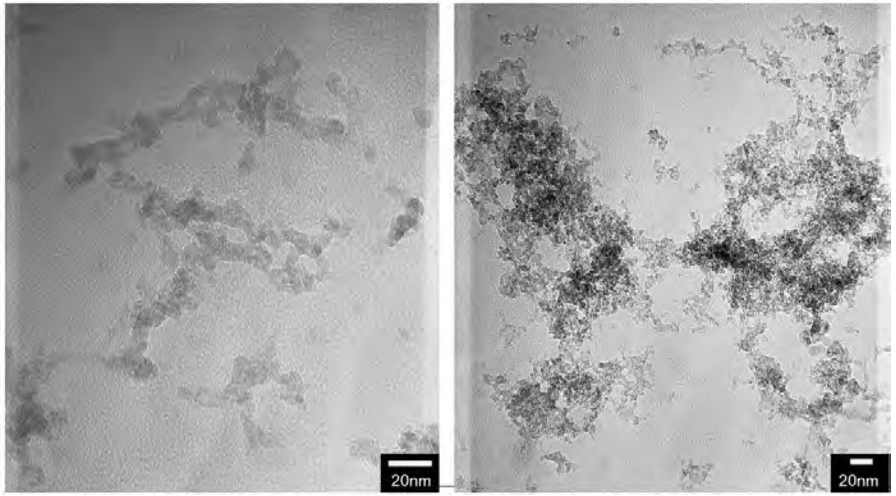

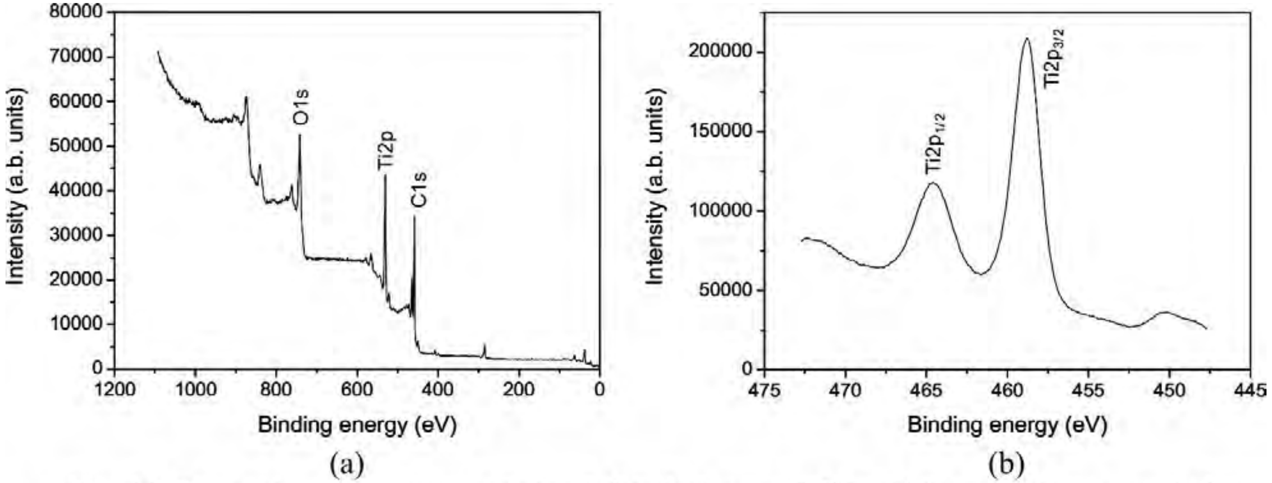

Fig. 4 XPS spectra of survey scan (a) and detailed scan of Ti2p (b) for sample nanoparticles.

Hyun Cheol Oh, Jun Ho Ji, Jae Hee Jung, and Sang Soo Kim. Synthesis of titania nanoparticles via spark discharge method using air as a carrier. In *Eco-Materials Processing and Design VIII*, volume 544 of *Materials Science Forum*, pages 143–146. Trans Tech Publications, 5 2007.

Developments

Output

XRD studies

2007

- 10 – 20 nm particles
- Collection by filtration

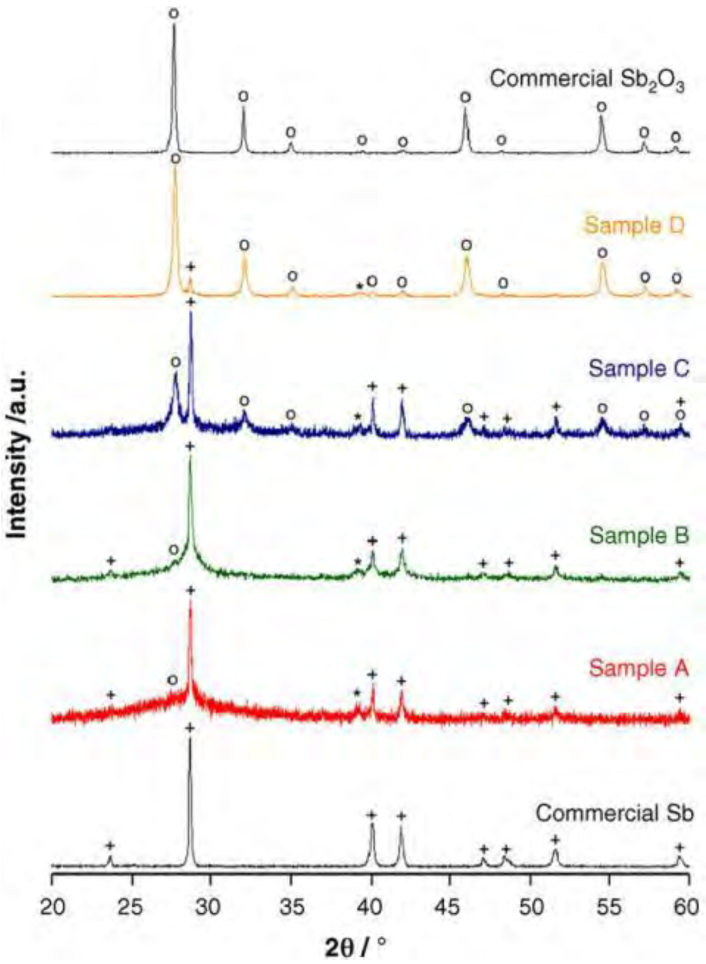

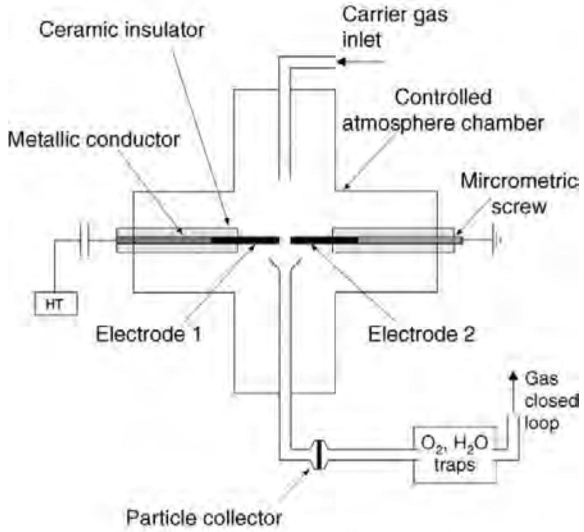

Fig. 1. Spark Discharge Generator.

L. Simonin, U. Lafont, N. Tabrizi, A. Schmidt-Ott, and E.M. Kelder. Sb/o nano-composites produced via spark discharge generation for li-ion battery anodes. *Journal of Power Sources*, 174(2):805 – 809, 2007. 13th International Meeting on Lithium Batteries.

vsparticle

Dylec 東京ダイレック株式会社

Developments

Output

Influence of nanoparticle material of size distributions

2008

- Precious metals in N_2 gas
- High production rates give higher concentrations and larger particles (Au > Pt > Pd > Ag)

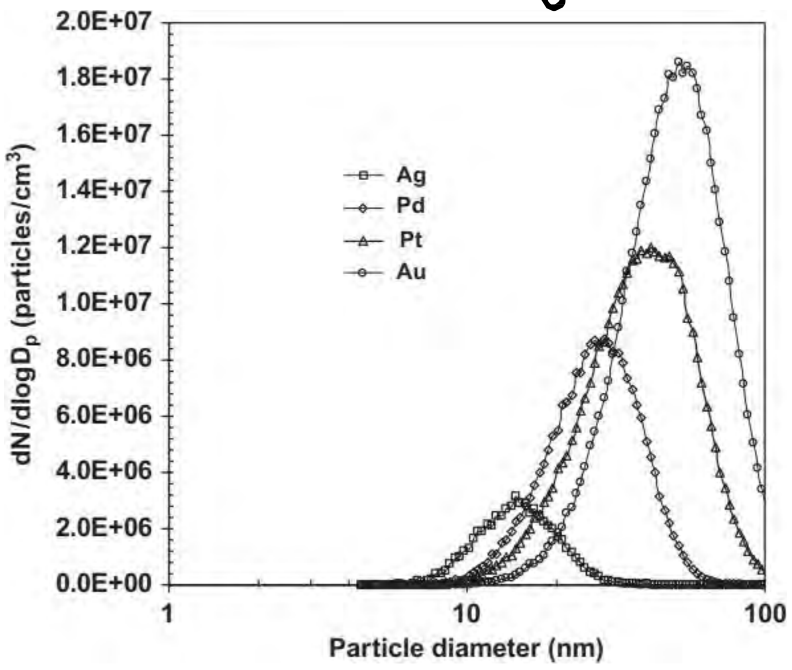

Jeong Hoon Byeon, Jae Hong Park, and Jungho Hwang. Spark generation of monometallic and bimetallic aerosol nanoparticles. *Journal of Aerosol Science*, 39(10):888 – 896, 2008.

Developments

Patterning

Patterning with metal catalyst particles

2008

- Pt particles in N_2 gas
- 5 min deposition using thermophoresis (ΔT)

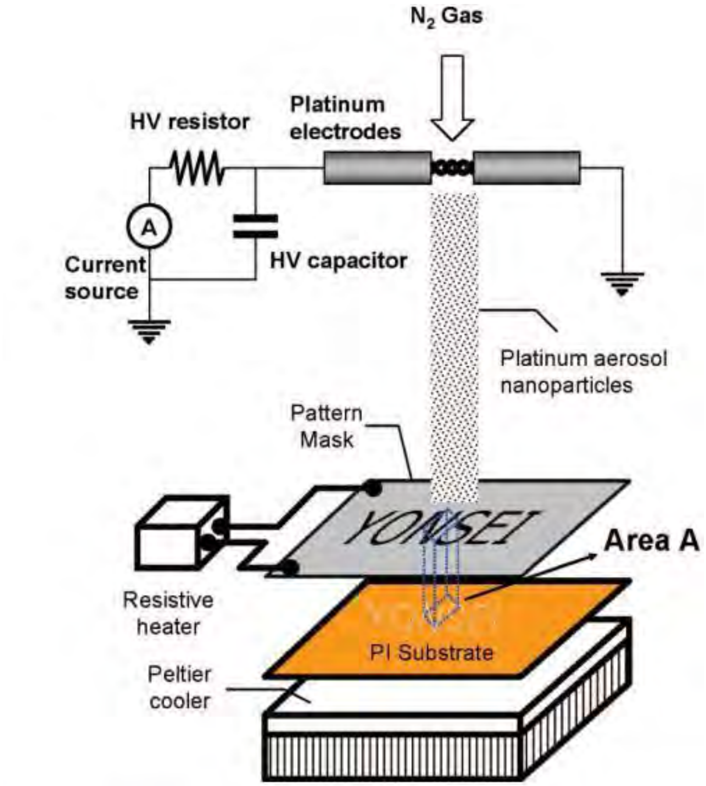

Figure 1. Overview of site-selective aerosol activation.

Jeong Hoon Byeon, Jae Hong Park, Ki Young Yoon, and Jungho Hwang. Site-selective catalytic surface activation via aerosol nanoparticles for use in metal micropatterning. *Langmuir*, 24(11):5949–5954, 2008.

vsparticle
Dylec 東京ダイレック株式会社

Developments

Material

Influence of carrier gas and various metals

2008

- Gases have various breakdown voltages
  changing the energy delivered to the spark
- Materials have different ablation rates depending on:
  - Thermal conductivity
  - Evaporation enthalpy
  - Boiling point

Table 1 Gold particle sizes under various conditions

	N_2		Ar		He	
P (atm)	1	2	1	2	1	2
d_g (nm)	7.0	5.5	4.7	4.7	4.0	4.1
σ_g	1.34	1.35	1.42	1.37	1.45	1.4
Count	35	37	40	44	69	36

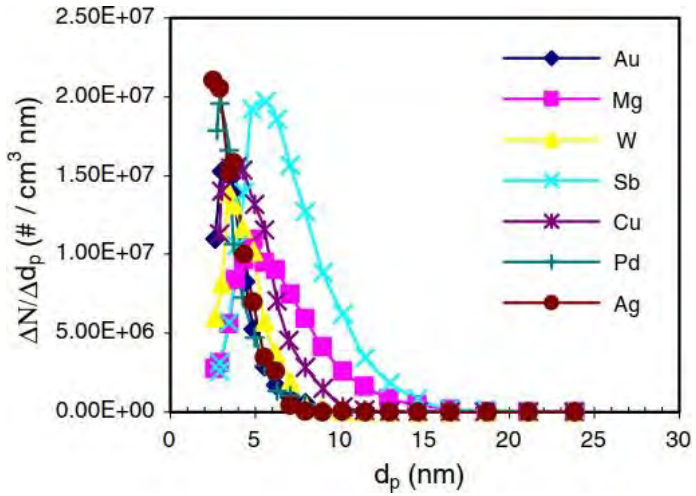

N. S. Tabrizi, M. Ullmann, V. A. Vons, U. Lafont, and A. Schmidt-Ott. Generation of nanoparticles by spark discharge. *Journal of Nanoparticle Research*, 11(2):315, May 2008.

Developments

Output

Carbon encapsulation

2009

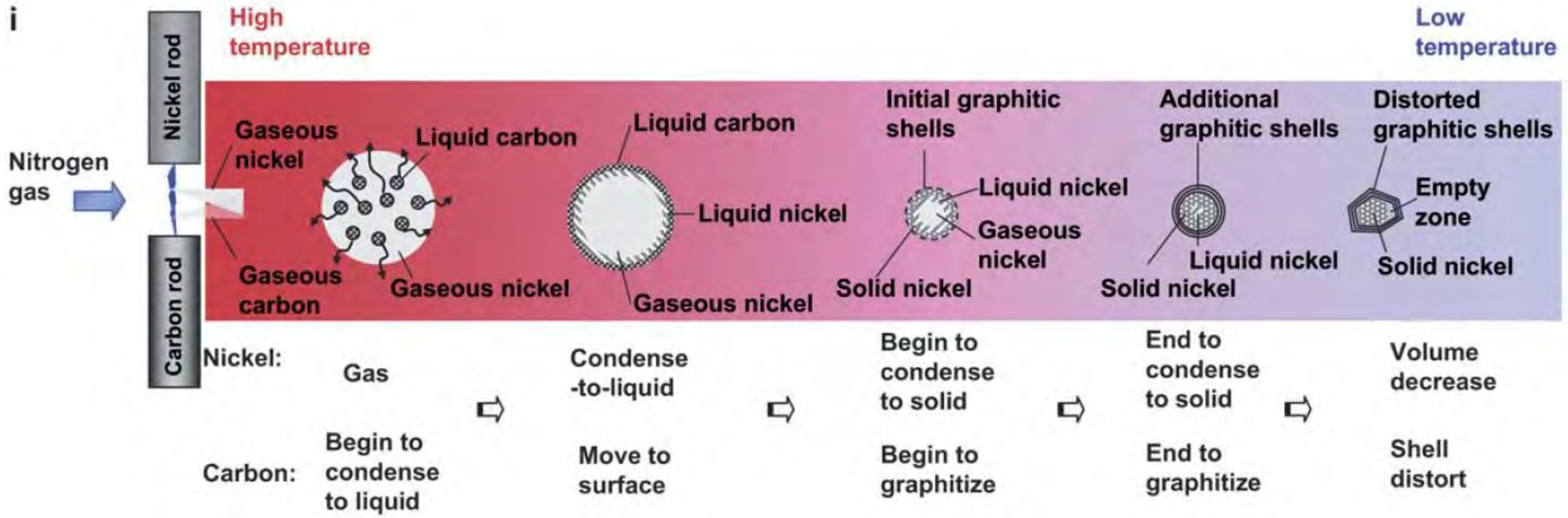

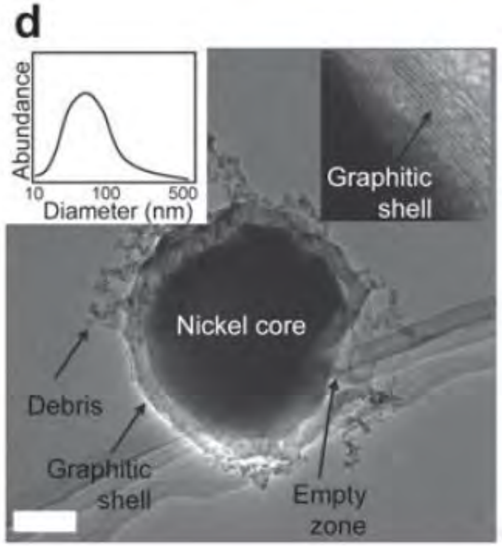

Jeong Hoon Byeon, Jae Hong Park, Ki Young Yoon, and Jungho Hwang. Ambient spark generation to synthesize carbon-encapsulated metal nanoparticles in continuous aerosol manner. *Nanoscale*, 1:339–343, 2009.

vsparticle
Dylec 東京ダイレック株式会社

Developments

Producing alloyed electrodes

Material

2009

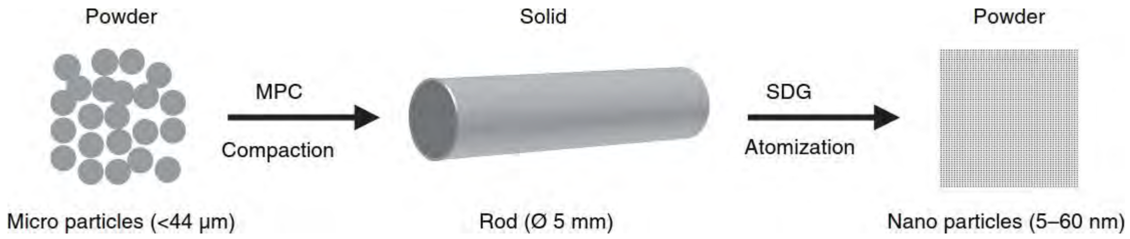

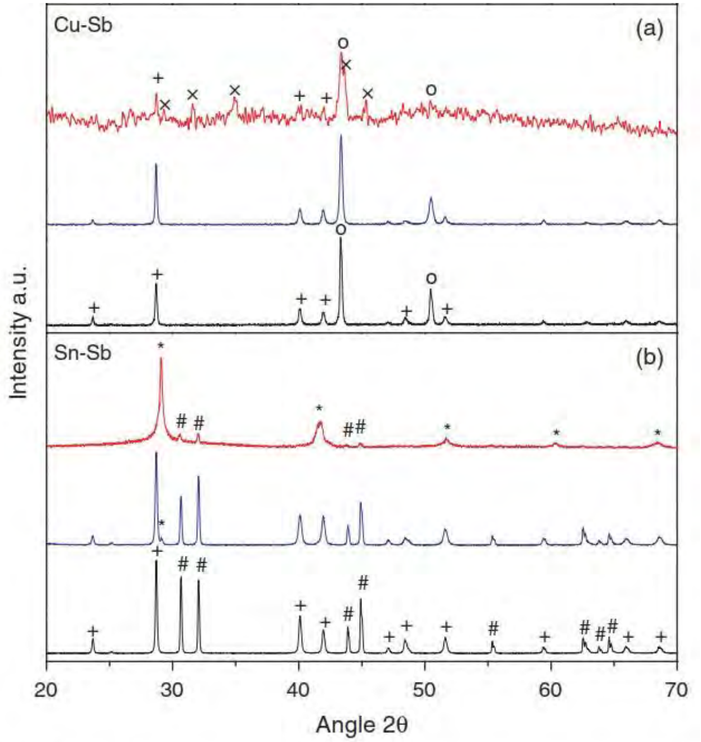

Fig. 8. (a) XRD pattern of the Cu-Sb sample before compaction (bottom, black), after compaction (middle, blue) and after atomization (top, red). # Sb phase, o Cu phase and $\times Cu_2Sb$ phase. (b) XRD pattern of the Sn-Sb sample before compaction (bottom, black), after compaction (middle, blue) and after atomization (top, red). # Sn phase, + Sb phase and $*$ SnSb phase.

Ugo Lafont, Loïc Simonin, Nooshin S. Tabrizi, Andreas Schmidt-Ott, and Erik M. Kelder. Synthesis of nanoparticles of cu, sb, sn, snsb and cu2sb by densification and atomization process. *Journal of Nanoscience and Nanotechnology*, 9(4):2546–2552, 2009.

Developments

Using nanoparticles as seeds for epitaxial growth

Application

2009

Deposition by electrostatic precipitation

Figure 4

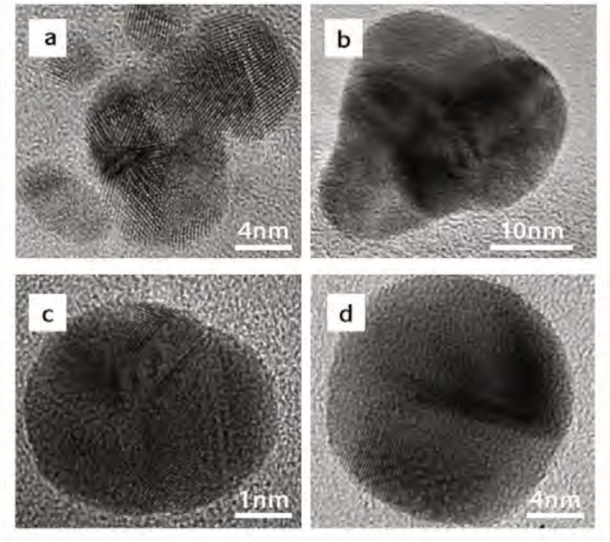

TEM micrographs of (a) agglomerate gold particles and gold particles reshaped at (b) 300°C (c) 600°C (d) 1200°C in a special compaction tube furnace

Figure 6

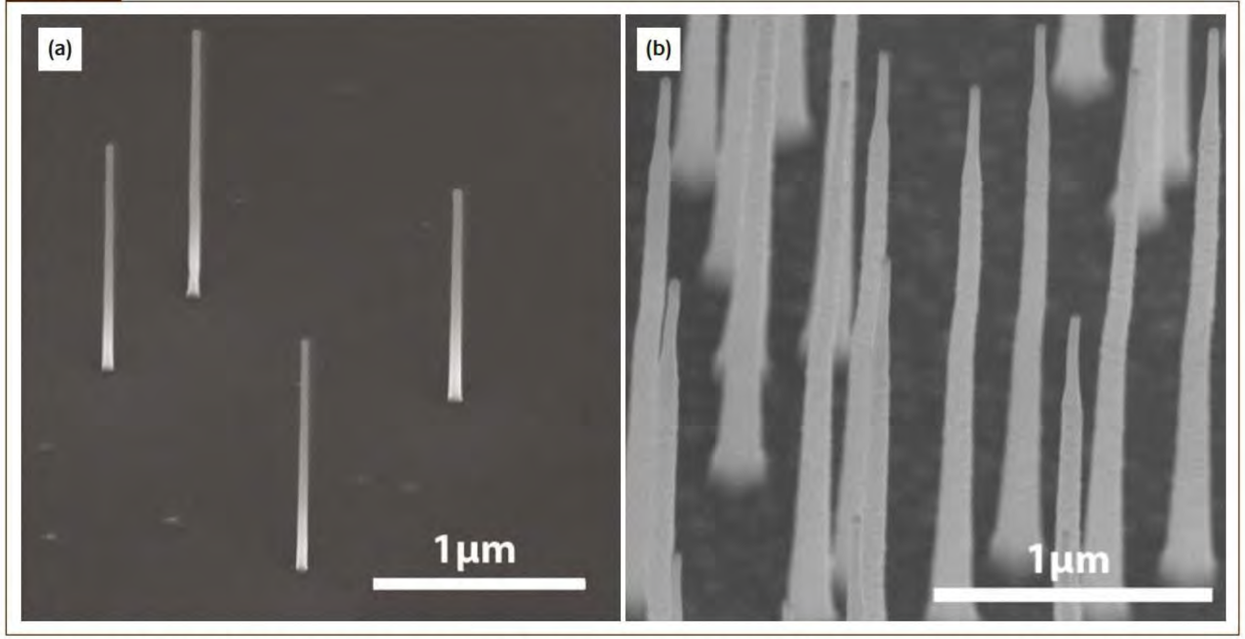

SEM micrograph of (a) epitaxial GaP nanowires seeded with 20 nm gold particles, reshaped at 600°C, at a growth temperature of 460°C. The particle density was 1 µm^{-2}. (b) epitaxial InP nanowires seeded with 30 nm gold particles, reshaped at 600°C, at a growth temperature of 420°C. The particle density was 3 µm^{-2}. Images were acquired with the sample tilted (a) 52° (b) 30° towards the e-beam

Maria E. Messing, Kimberly A. Dick, L. Reine Wallenberg, and Knut Deppert. Generation of size-selected gold nanoparticles by spark discharge — for growth of epitaxial nanowires. *Gold Bulletin*, 42(1):20–26, Mar 2009.

Developments

Application

Study of model catalysts using aerosol deposition

2010

- Size selected Pd nanoparticles
- Deposition on Si by electrostatic precipitation

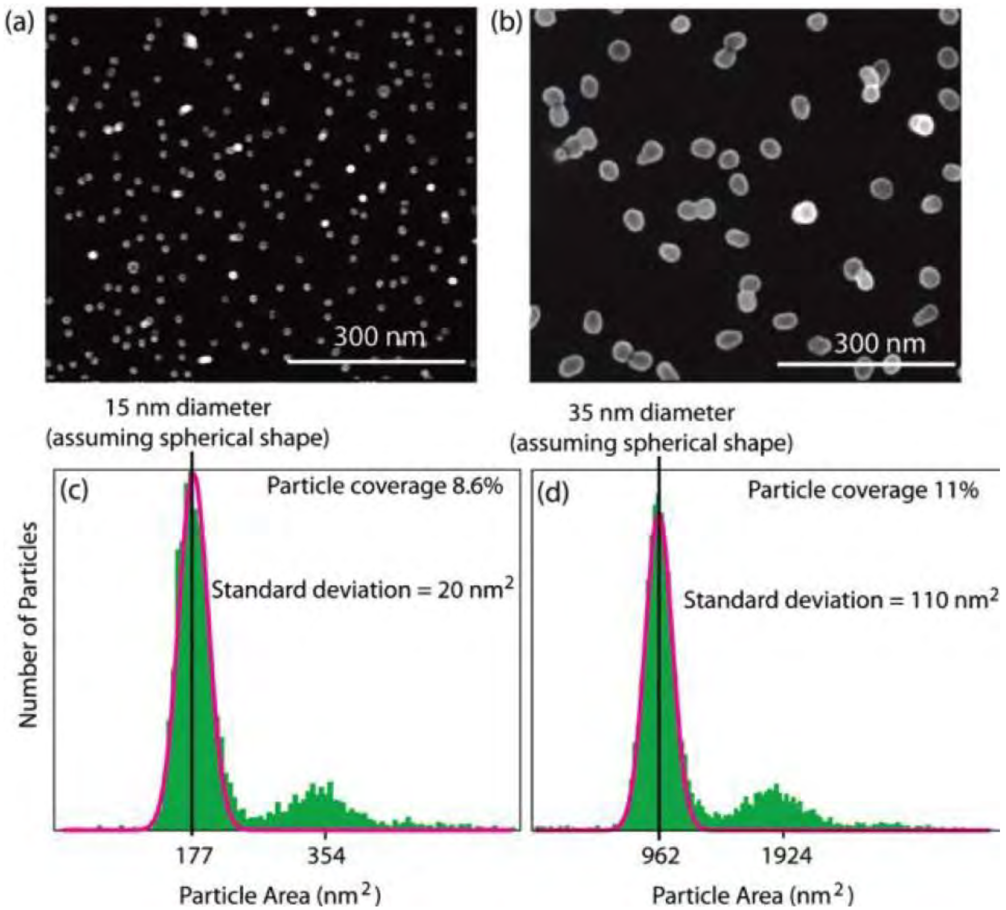

Maria E. Messing, Rasmus Westerström, Bengt O. Meuller, Sara Blomberg, Johan Gustafson, Jesper N. Andersen, Edvin Lundgren, Richard van Rijn, Olivier Balmes, Hendrik Bluhm, and Knut Deppert. Generation of pd model catalyst nanoparticles by spark discharge. *The Journal of Physical Chemistry C*, 114(20):9257–9263, 2010.

Developments

Material

Metallic nanoparticles from immiscible metals

2010

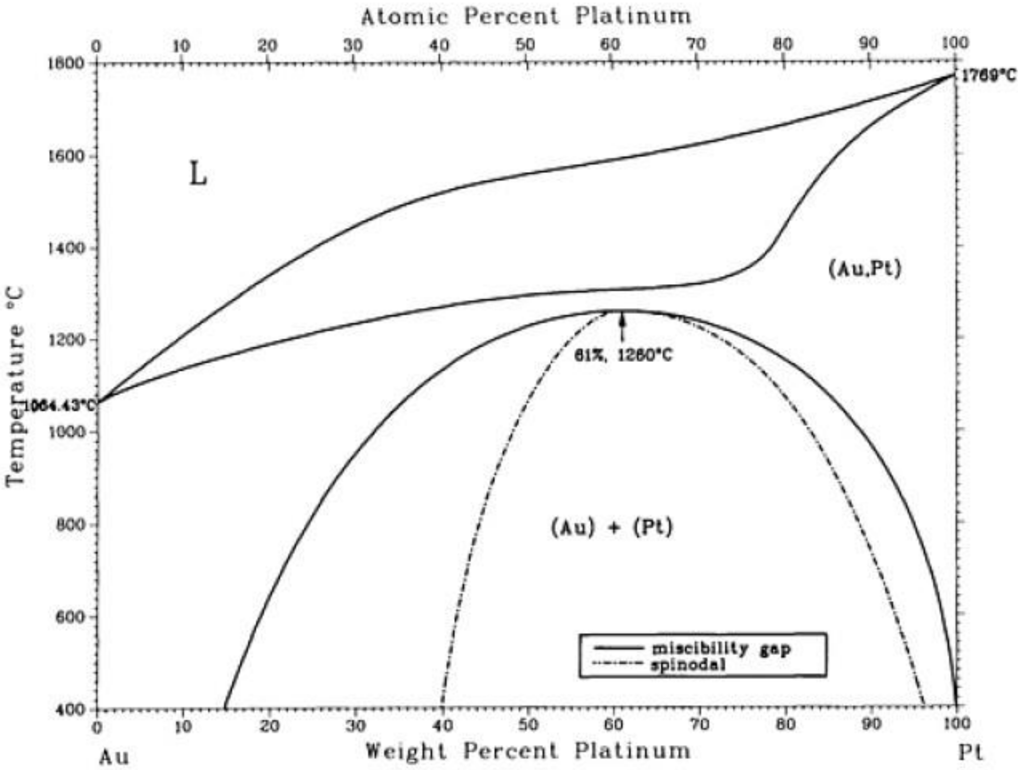

Fig. 6 EDS compositional mapping of the specified Au–Pt particle ~6 nm in size (**a**), Au L (**b**) and Pt L (**c**)

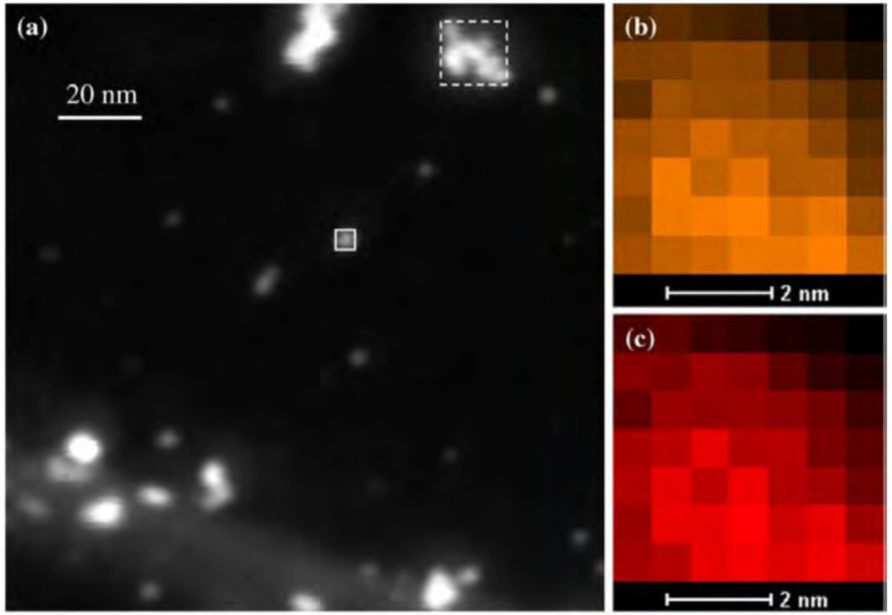

N. S. Tabrizi, Q. Xu, N. M. van der Pers, and A. Schmidt-Ott. Generation of mixed metallic nanoparticles from immiscible metals by spark discharge. *Journal of Nanoparticle Research*, 12(1):247–259, Jan 2010.

vsparticle

Dylec 東京ダイレック株式会社

Developments

Semiconducting nanoparticles

Material

2011

- Doping decreases electrical resistivity (0.17 Ω cm)

  10^{15} boron atoms/cm^3

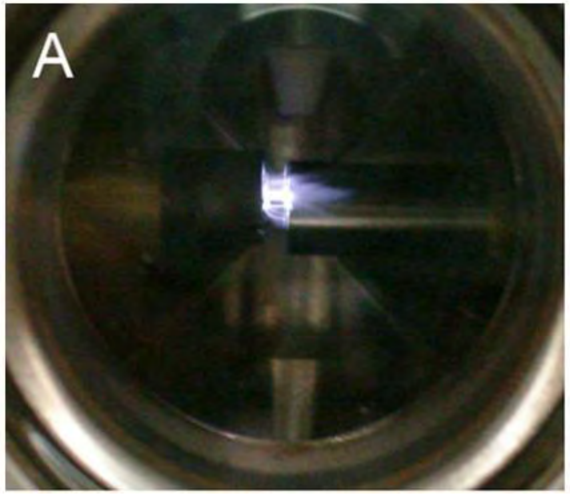

Fig. 5 **a** Photographs of an intrinsic silicon discharge.

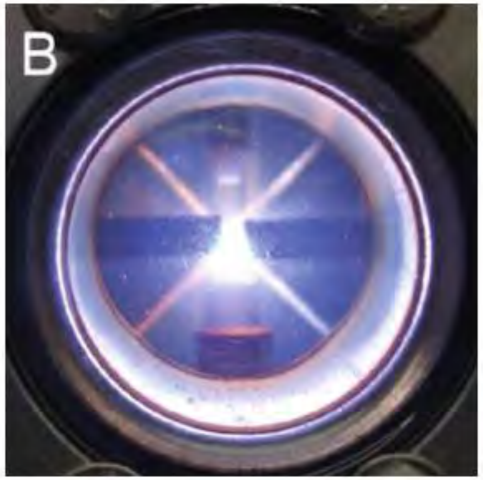

Fig. 7 **a** Discharge voltage and current for boron-doped Si rods in 1.6 SLM Ar 5.0, 2 mm gap spacing. **b** photograph of the spark discharge between doped rods

Vincent A. Vons, Louis C. P. M. de Smet, David Munao, Alper Evirgen, Erik M. Kelder, and Andreas Schmidt-Ott. Silicon nanoparticles produced by spark discharge. *Journal of Nanoparticle Research*, 13(10):4867, Jun 2011.

Developments

Output

Deposition of uniform layers

2011

- Deposition of Ag nanoparticles by diffusion
- Annealing at 300 C for 30 min
- Layer height of 104 nm
- Surface roughness of 8.7 nm

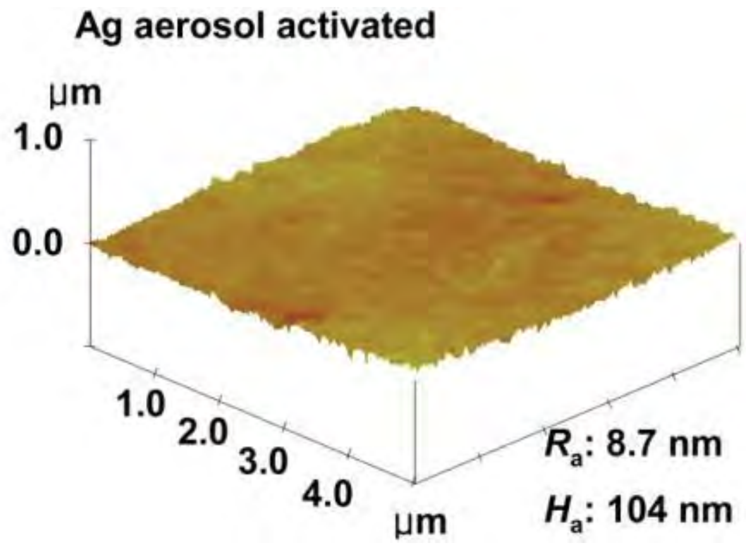

Jeong Hoon Byeon and Jang-Woo Kim. Fabrication of a pure, uniform electroless silver film using ultrafine silver aerosol particles. *Langmuir*, 26(14):11928–11933, 2010.

vsparticle

Dylec 東京ダイレック株式会社

Developments

Material

Production of highly oxidizing metals

2011

- Production of Mg nanoparticles
- Purification of 5N Ar: 5 ppm H_2O, O_2
- Bake-out of the system
- Preloading of the system with Mg NPs

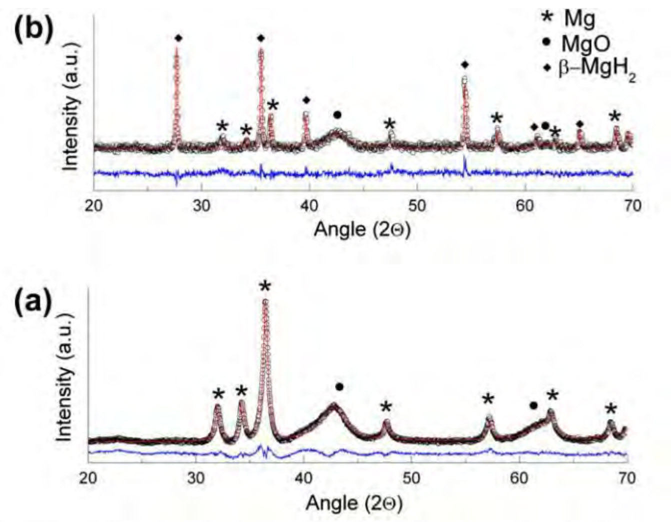

Fig. 4. XRD patterns of Mg nanoparticles after background substraction: (a) as-produced; (b) after hydrogen loading (black, measured spectrum; red, Rietveld analysis; blue, residual of the fit). (For interpretation of the references to colour in this figure legend, the reader is referred to the web version of this article.)

V.A. Vons, A. Anastasopol, W.J. Legerstee, F.M. Mulder, S.W.H. Eijt, and A. Schmidt-Ott. Low-temperature hydrogen desorption and the structural properties of spark discharge generated mg nanoparticles. *Acta Materialia*, 59(8):3070 – 3080, 2011.

vsparticle

Dylec 東京ダイレック株式会社

Developments

Output

Size selected deposition of Au, Ge

2012

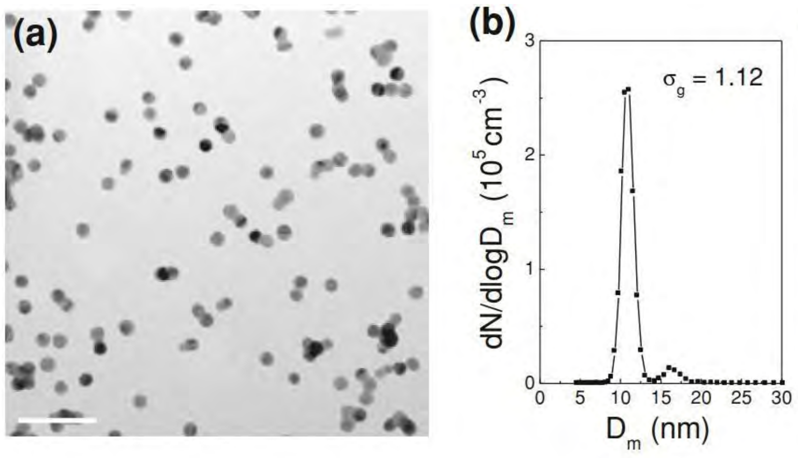

Fig. 4.7 **a** Bright field TEM images of Au nanoparticles of geometric mean diameter of 9.87 nm, **b** size distribution by SMPS measurement and **c** size distribution calculated by TEM images

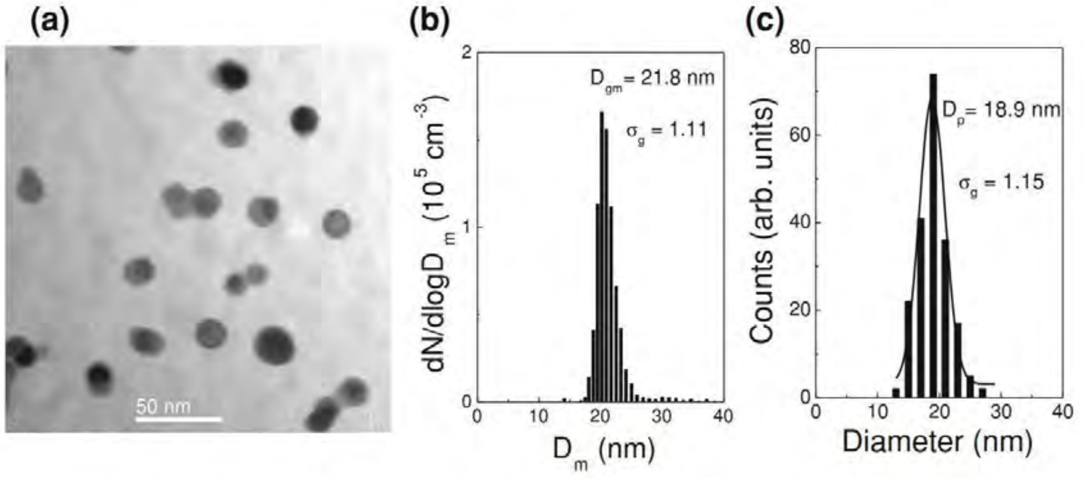

Fig. 4.10 **a** TEM image of Ge nanoparticles, obtained after sintering at 900 °C, **b** size distribution as monitored by SMPS and **c** size distribution obtained by TEM images analysis

Shubhra Kala, Marcel Rouenhoff, Ralf Theissmann, and Frank Einar Kruis. *Synthesis and Film Formation of Monodisperse Nanoparticles and Nanoparticle Pairs*, pages 99–119. Springer Berlin Heidelberg, Berlin, Heidelberg, 2012.

vsparticle
Dylec 東京ダイレック株式会社

Developments

Writing by electrostatic focussing

Patterning

2012

- 10 nm Au particles on carbon

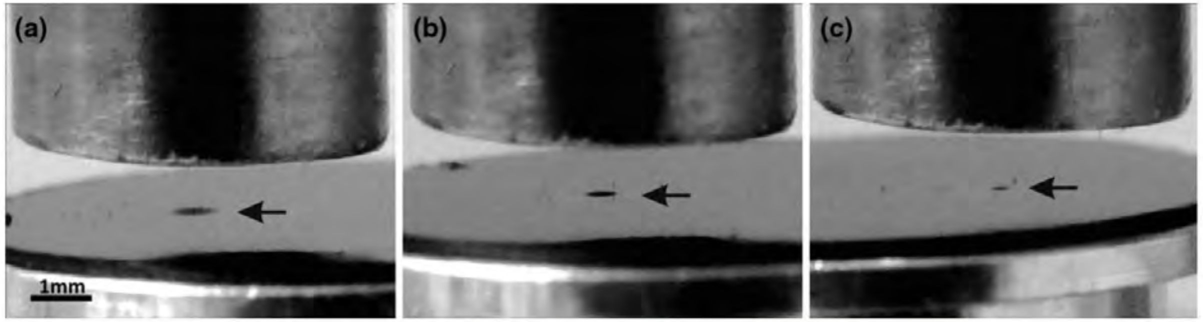

Fig. 9 Deposited spots using a 400 V focusing tube, b 1200 V focusing tube and c 1800 V focusing tube

Fig. 10 Intensity profiles of deposited spot images for different tube voltages

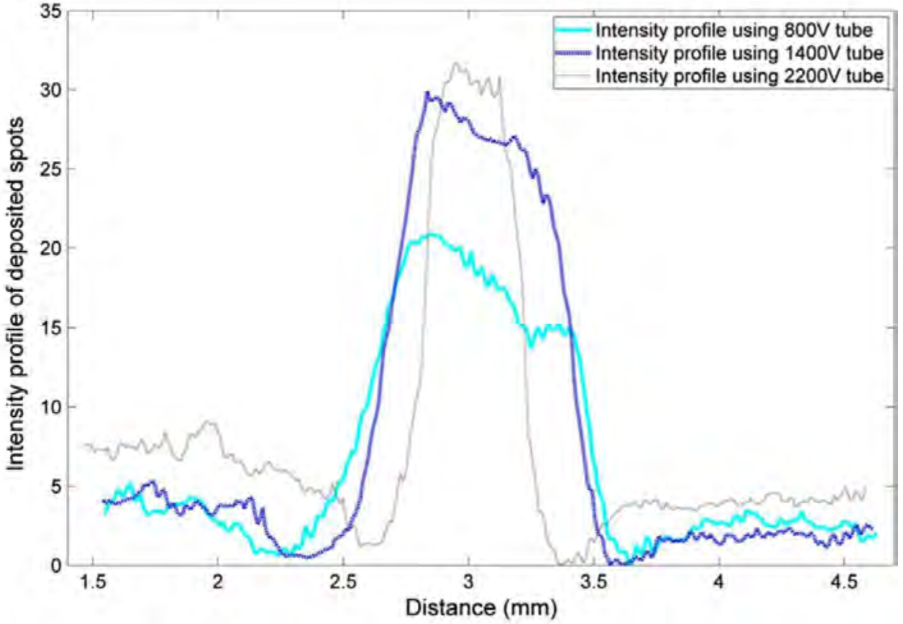

E. Saleh, M. Praeger, A. S. Vaughan, W. Stewart, and W. H. Loh. The direct writing and focusing of nanoparticles generated by an electrical discharge. *Journal of Nanoparticle Research*, 14(11):1220, Oct 2012.

Developments

Technical

Effect of different configurations

2012

- Configurations have different electrical fields and gas flow profiles

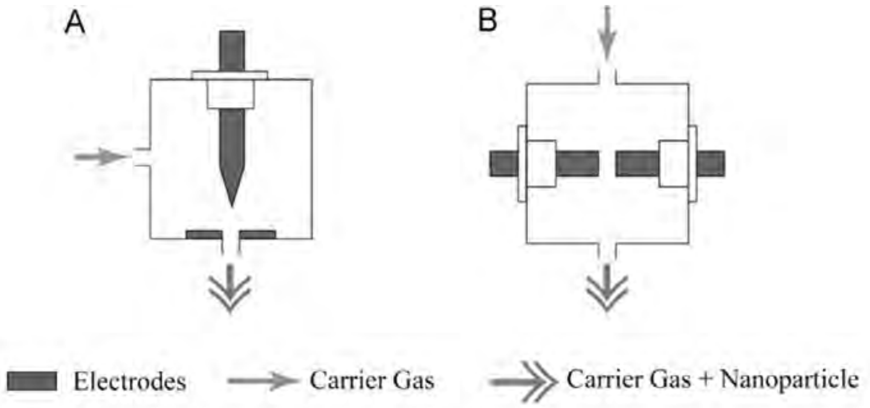

Fig. 1. Two different configurations of spark discharge generator. (A) Pin-to-plate type electrode configuration. (B) Rod-to-rod type electrode configuration.

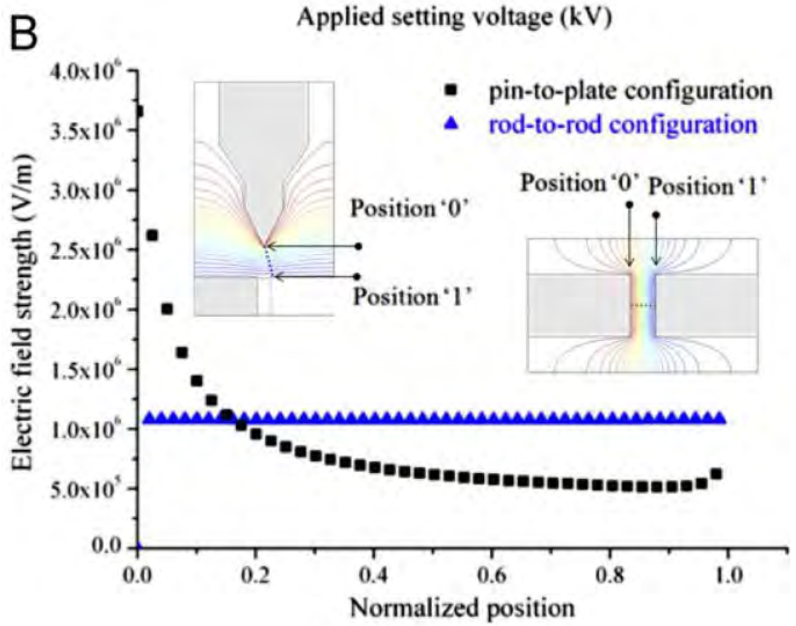

Kyuhee Han, Woongsik Kim, Jiwon Yu, Jeonghoon Lee, Heechul Lee, Chang Gyu Woo, and Mansoo Choi. A study of pin-to-plate type spark discharge generator for producing unagglomerated nanoaerosols. *Journal of Aerosol Science*, 52:80 – 88, 2012.

vsparticle

Dylec 東京ダイレック株式会社

Developments

High stability by thiol capping of Au NPs

2012

Scheme 1. Aerosol Based Fabrication of Thiol-Capped Au Nanoparticles

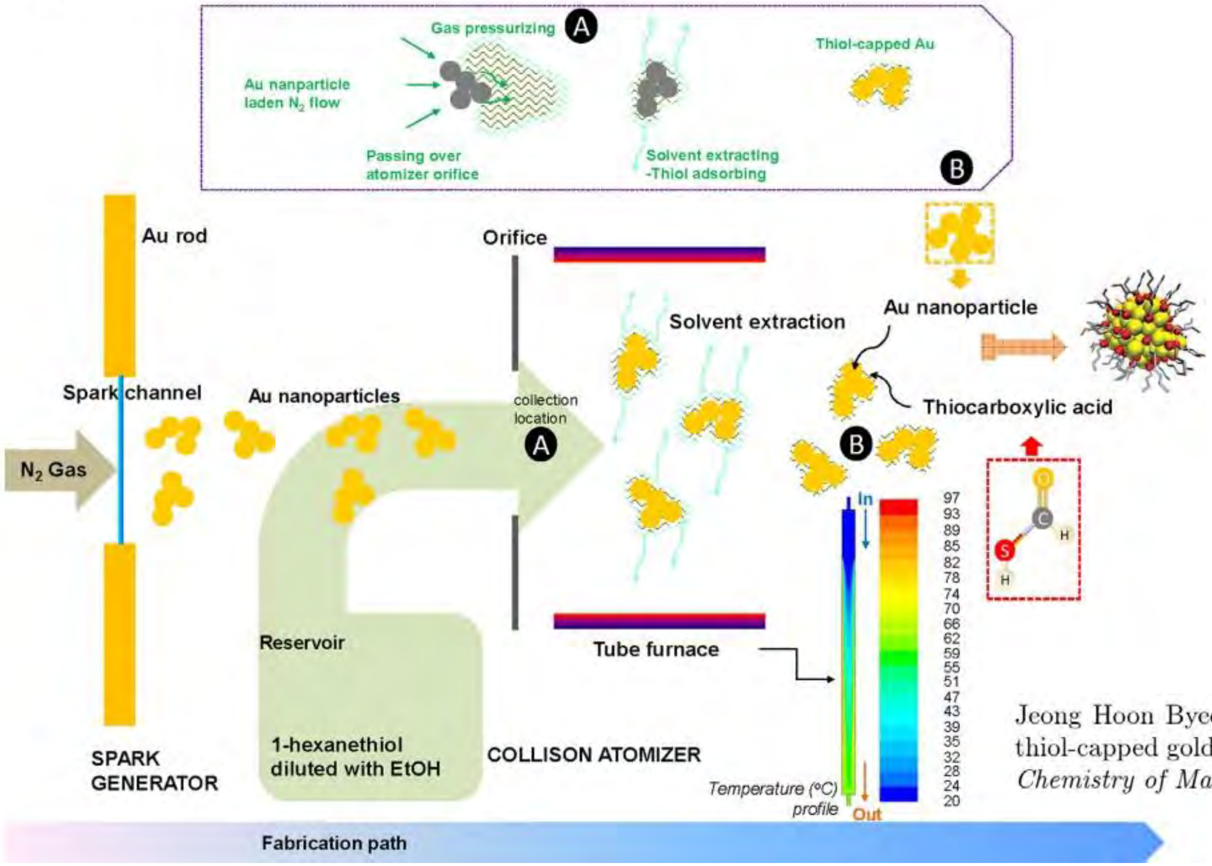

Jeong Hoon Byeon and Jeffrey T. Roberts. Aerosol based fabrication of thiol-capped gold nanoparticles and their application for gene transfection. *Chemistry of Materials*, 24(18):3544–3549, 2012.

Developments

Production of large spherical particles

2012

- Particles > 10 nm tend to agglomerate
- Higher temperature increases mobility and produces spherical particles

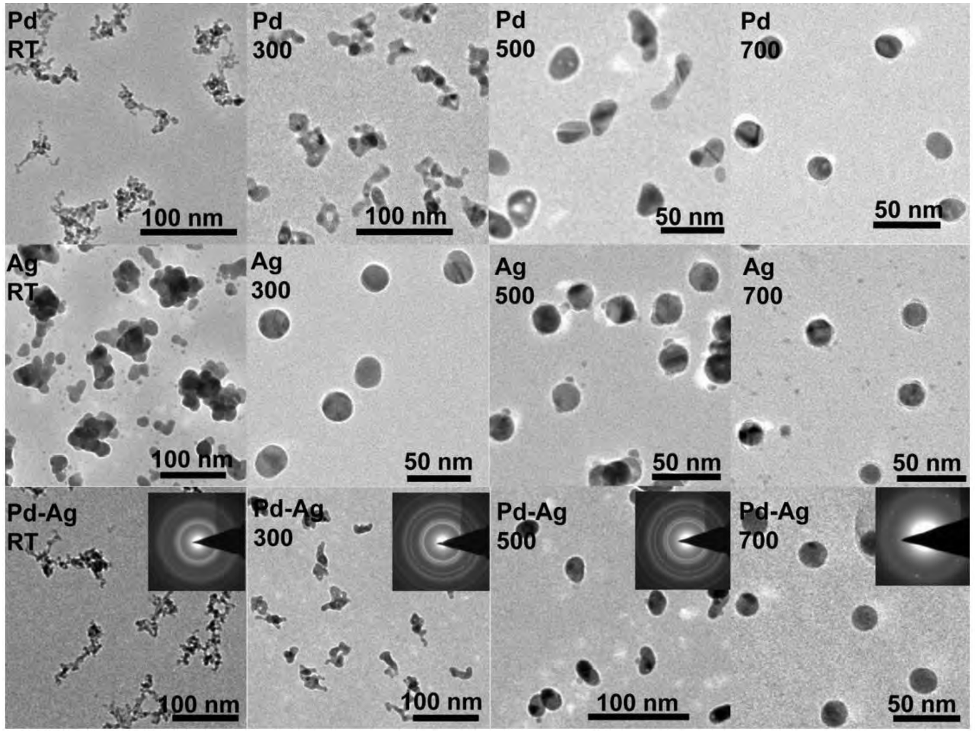

FIG. 2. TEM micrographs of the Pd, Ag, and Pd-Ag alloy nanoparticles sintered at RT, 300 °C, 500 °C, and 700 °C.

Saurabh K. Sengar, B. R. Mehta, and Govind. Size and alloying induced changes in lattice constant, core, and valance band binding energy in pd-ag, pd, and ag nanoparticles: Effect of in-flight sintering temperature. *Journal of Applied Physics*, 112(1):014307, 2012.

vsparticle

Dylec 東京ダイレック株式会社

Developments

Titania nanoparticles for photocatalysis

2013

Scheme 1. Continuous Gas-Phase Self-Assembly of Graphene Nanoflakes with TiO_2 Nanoparticles for Photocatalytic Applications; Other Nanoparticles (ZnO, Au, and Ag) were Also Incorporated with Graphene Nanoflakes via the Same Method

- Spark ablation under air stream
- Deposition on graphene

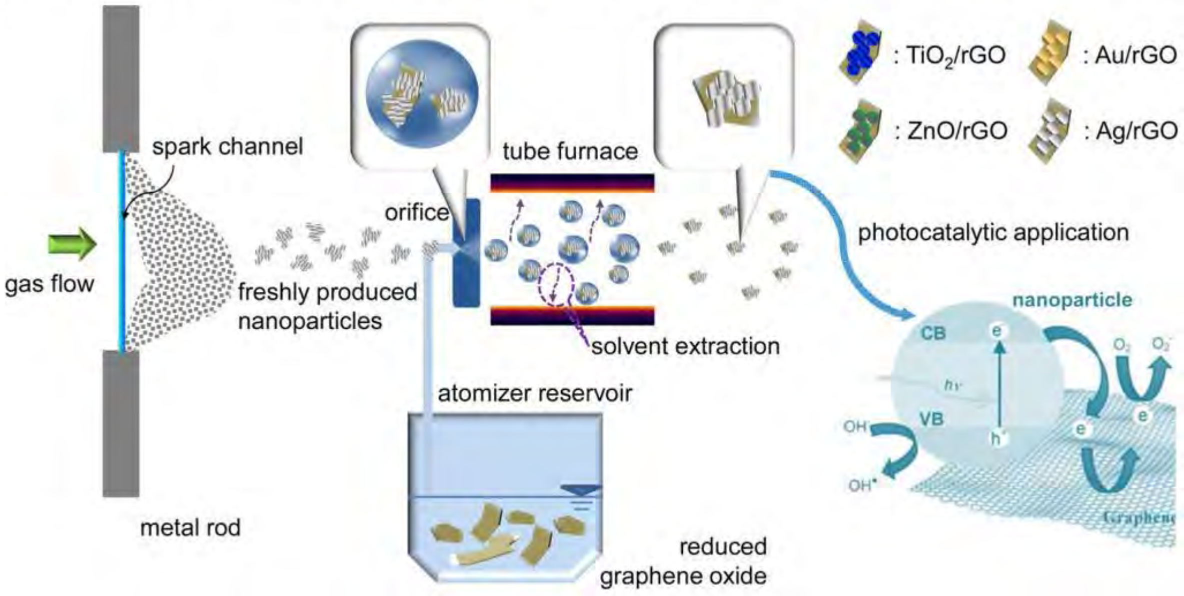

Jeong Hoon Byeon and Young-Woo Kim. Gas-phase self-assembly of highly ordered titania@graphene nanoflakes for enhancement in photocatalytic activity. *ACS Applied Materials & Interfaces*, 5(9):3959–3966, 2013.

vsparticle

Dylec 東京ダイレック株式会社

Developments

Antibacterial silver coatings on HEPA filters

2013

- Dust captured in filters can serve as nutrients for bacteria
- Ag limits growth

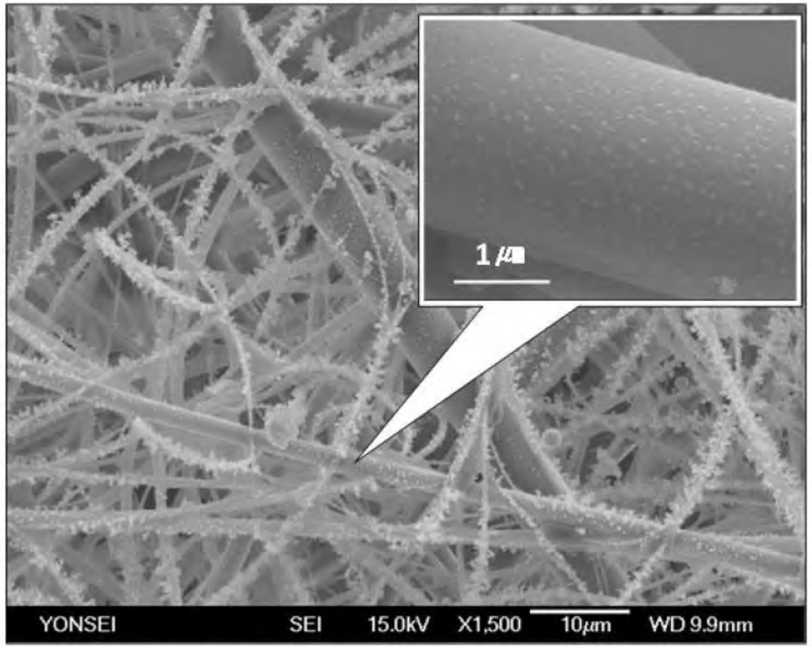

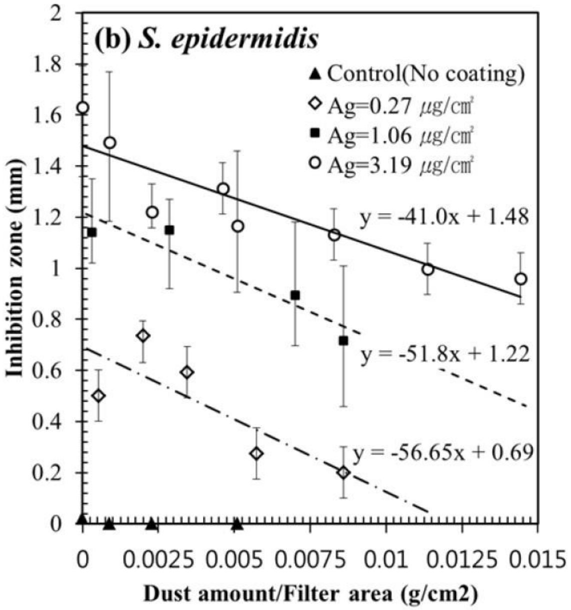

Fig. 2. FESEM photograph of the silver-deposited HEPA filter with no dust loading (coating time is 60 min).

Yun Haeng Joe, Wei Ju, Jae Hong Park, Young Hun Yoon, and Jungho Hwang. Correlation between the antibacterial ability of silver nanoparticle coated air filters and the dust loading. *Aerosol and Air Quality Research*, 13(3):1009–1018, 2013.

vsparticle

Dylec 東京ダイレック株式会社

Developments

Growth of superstructures

2013

- Nanosecond spark duration
- Mo in air
- Deposition of MoO_3 on Cu foil 3 mm from spark

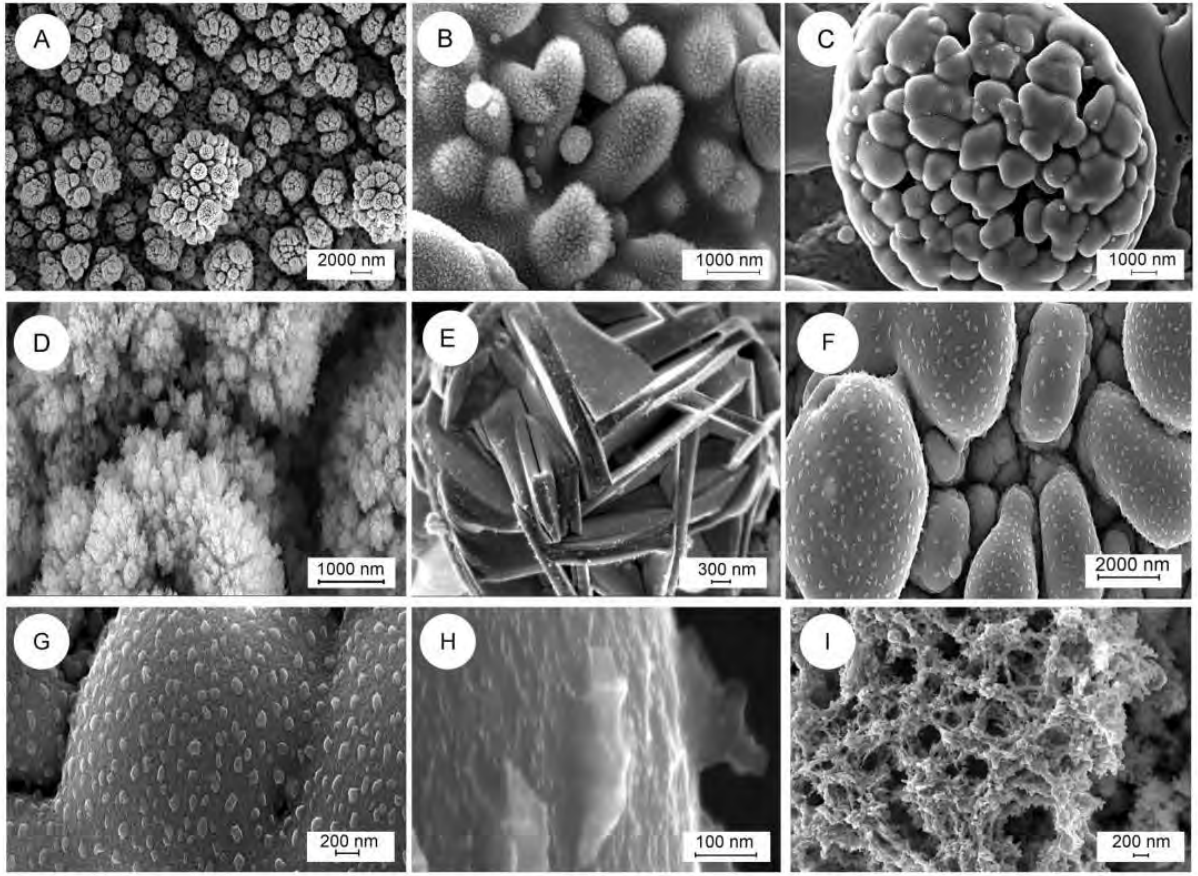

Figure 3 | SEM images of MoO_3 nanostructures. (a–e) Deposited in the pin-to-pin electrode configuration, (f–h) deposited in the pin-to-plate electrode configuration; (i) porous networks of MoO_3 deposited in the pin-to-plate configuration.

- Nanoparticles
- Nanoflakes
- Nanowalls
- Nanocrystals
- Nanotubes

David Z. Pai, Kostya (Ken) Ostrikov, Shailesh Kumar, Deanna A. Lacoste, Igor Levchenko, and Christophe O. Laux. Energy efficiency in nanoscale synthesis using nanosecond plasmas. *Scientific Reports*, 3:1221 EP –, Feb 2013. Article.

vsparticle
Dylec 東京ダイレック株式会社

Developments

Synthesis of hollow NPs

2014

- Si around molten Fe
- Fe diffuses inside Si because of temperature gradient

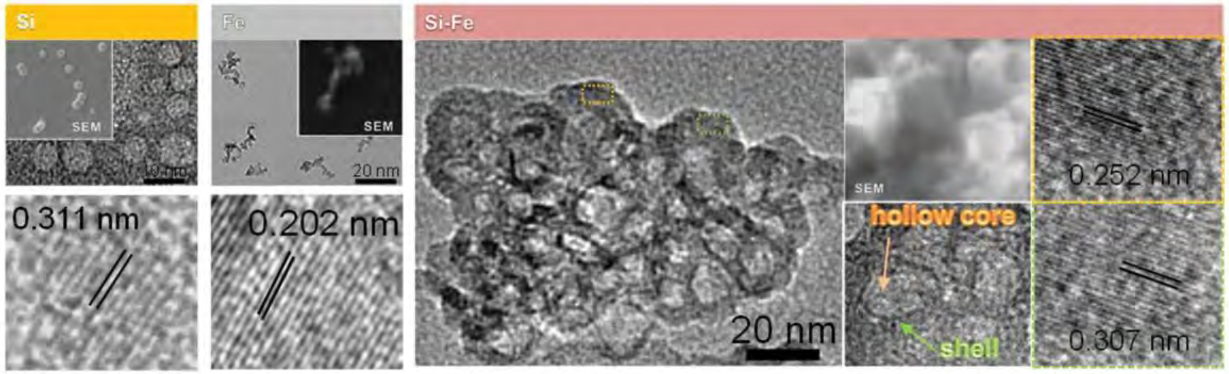

Figure 2. Low- and high-magnification TEM images of individual Si (8.8 ± 2.3) and Fe (26.1 ± 7.9) particles, and their incorporated nanostructures (Si-Fe, 21.8 ± 2.6). Representative SEM images of each sample are also displayed.

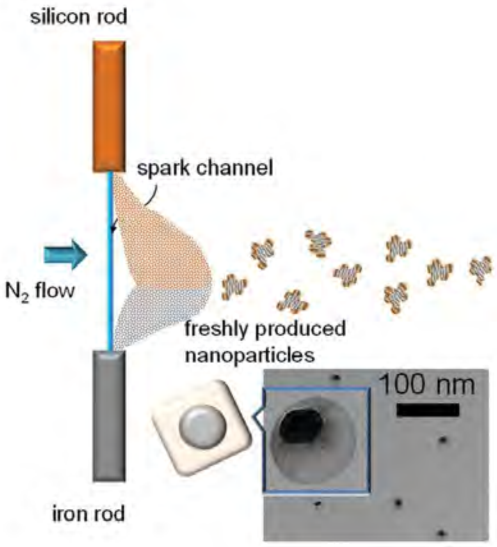

Jeong Hoon Byeon and Young-Woo Kim. Ambient plasma synthesis of si-fe hollow nanoparticles and their biocompatibility and lithium storage capacity. *Advanced Materials Interfaces*, 1(5):1300134, 2014.

Developments

Increased production rate by increasing the frequency

2014

- Standard operation: 200 Hz (0.3 mg Cu / h)
- Large scale: 10 kHz (30 mg Cu / h)

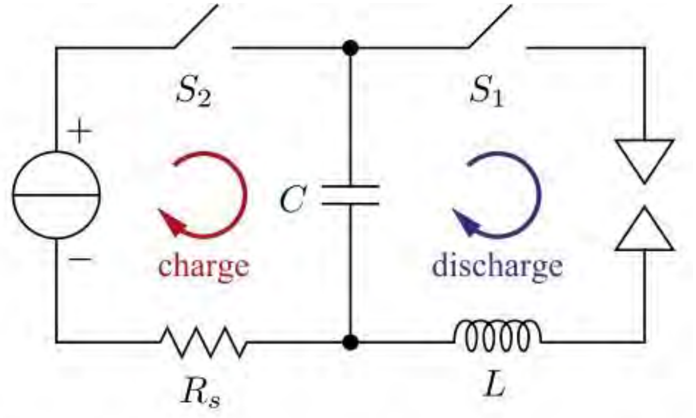

Fig. 5.2. Decoupling charge and discharge cycles.

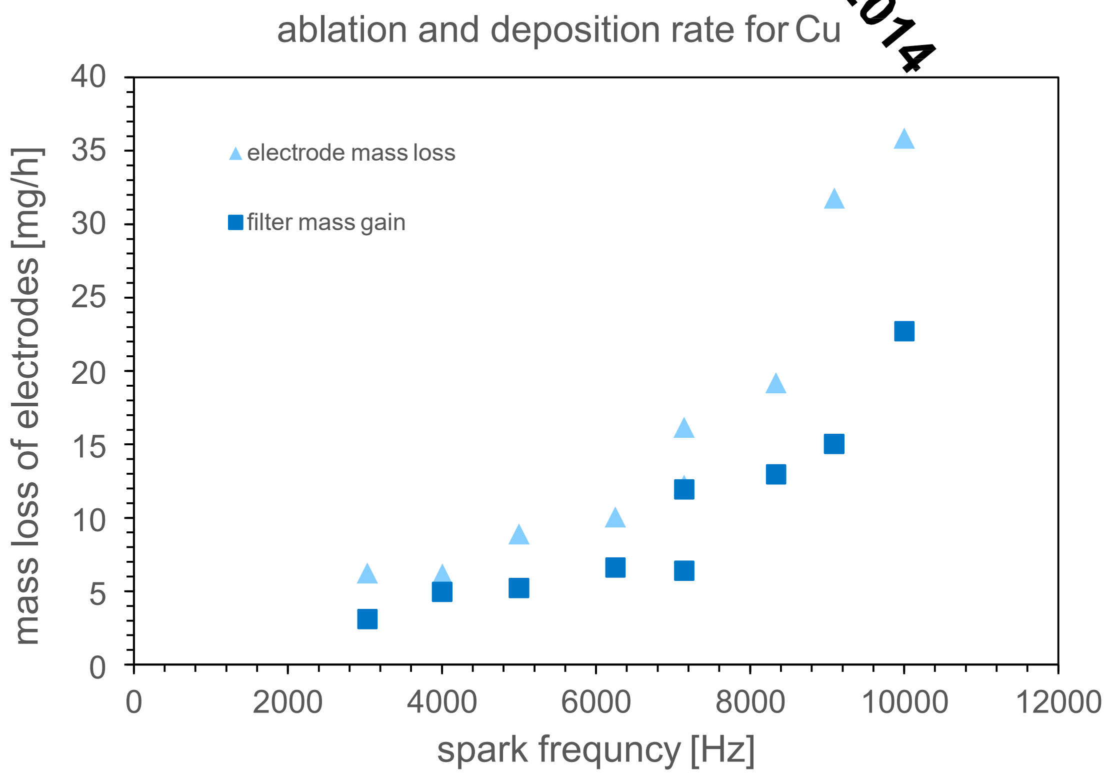

T.V. Pfeiffer, J. Feng, and A. Schmidt-Ott. New developments in spark production of nanoparticles. *Advanced Powder Technology*, 25(1):56 – 70, 2014.

vsparticle

Dylec 東京ダイレック株式会社

Developments

Spark behavior in time

2015

- Spark behavior depends:
  - Electrode geometry
  - Electrode gap
  - Gas flow rate

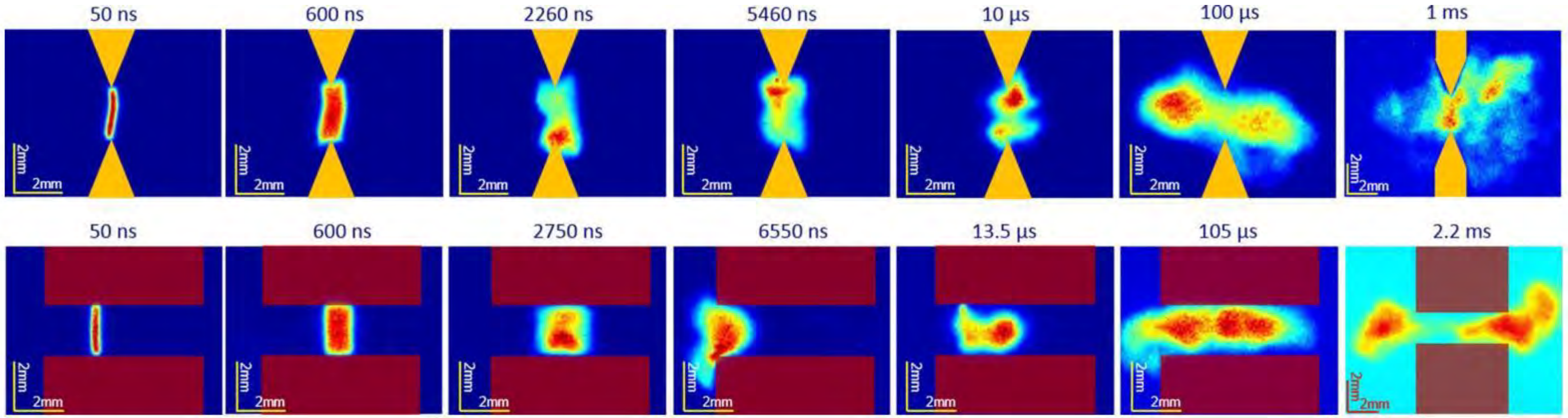

FIG. 5. Images acquired at different delays for spark discharges between tipped-end (upper row) and flat-end (lower row) electrodes placed at 2 mm distance in 10 slm of co-axial N_2 flow. The spark energy was 224 and 427 mJ for the tipped- and flat-end electrodes, respectively. The top electrode was initially the anode in both cases.

J. M. Palomares, A. Kohut, G. Galbács, R. Engeln, and Zs. Geretovszky. A time-resolved imaging and electrical study on a high current atmospheric pressure spark discharge. *Journal of Applied Physics*, 118(23):233305, 2015.

Developments

Patterning by electrostatic focusing

2015

- Patterning by floating metal mask

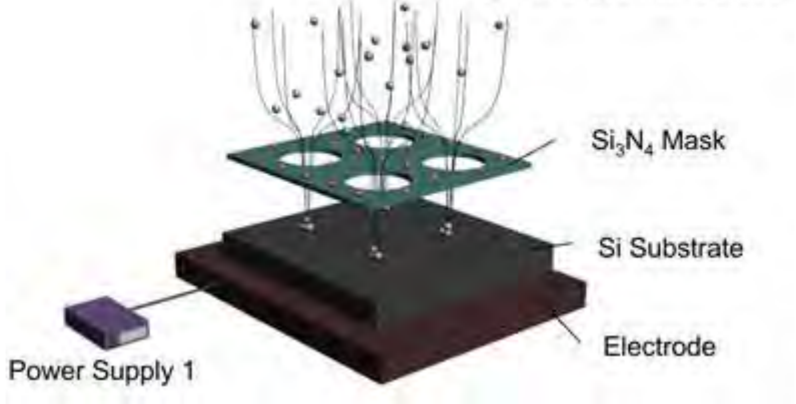

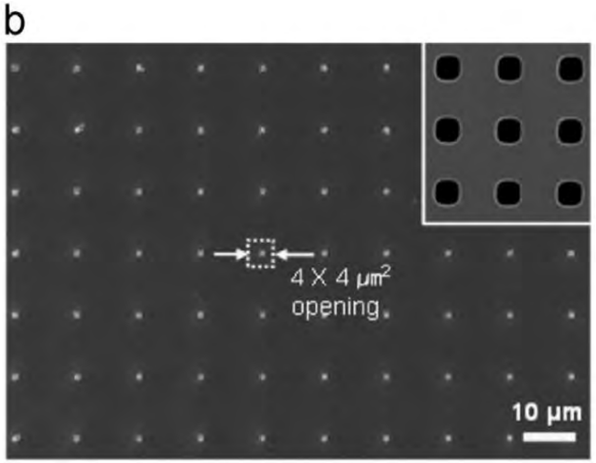

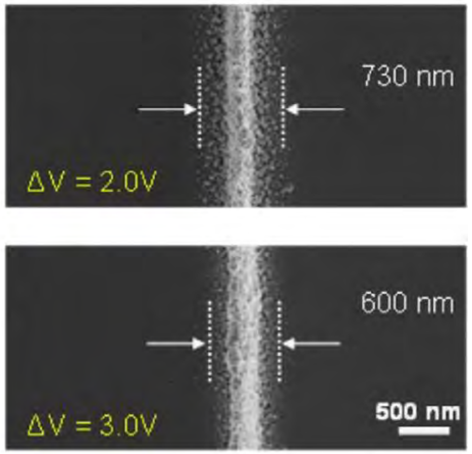

Hoseop Choi, Seunghyon Kang, Wooik Jung, Yoon ho Jung, Sei Jin Park, Dae Seong Kim, and Mansoo Choi. Controlled electrostatic focusing of charged aerosol nanoparticles via an electrified mask. *Journal of Aerosol Science*, 88:90 – 97, 2015.

vsparticle
Dylec 東京ダイレック株式会社

Developments

Particle size distributions from TEM data

2015

- Direct observation of Au particle size distributions by TEM
- Comparison of initial size and reference downstream

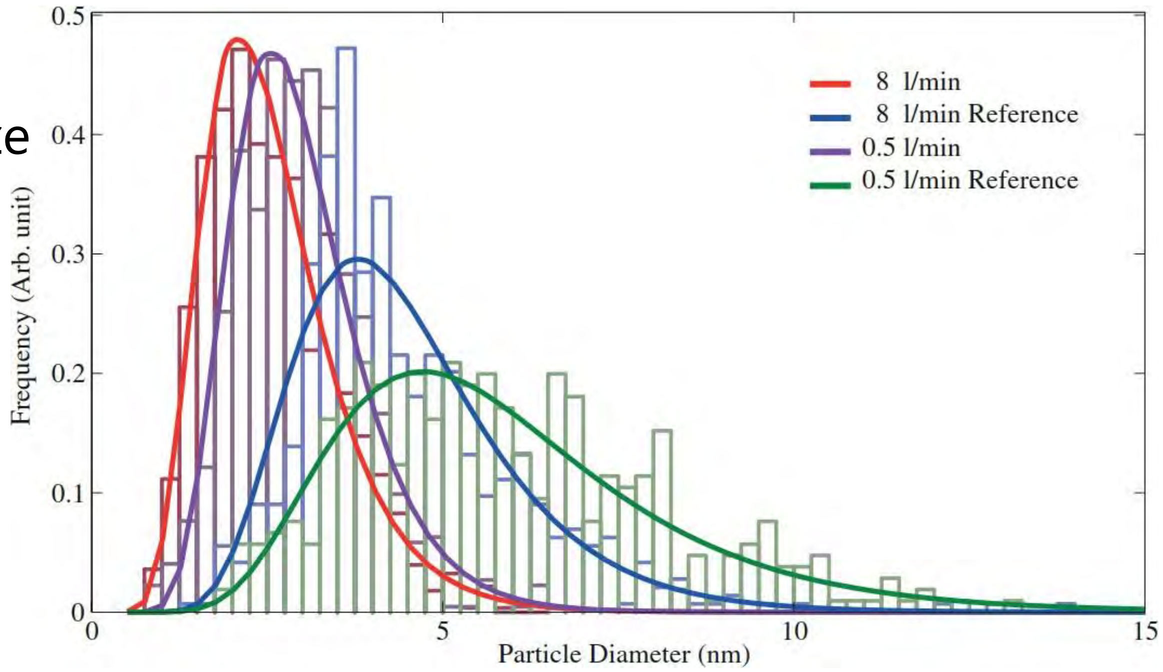

Linus Ludvigsson, Bengt O Meuller, and Maria E Messing. Investigations of initial particle stages during spark discharge. *Journal of Physics D: Applied Physics*, 48(31):314012, jul 2015.

Developments

Synthesis of single-walled carbon nanotubes

2015

- Growth of SWCNT by Fe NP seeding

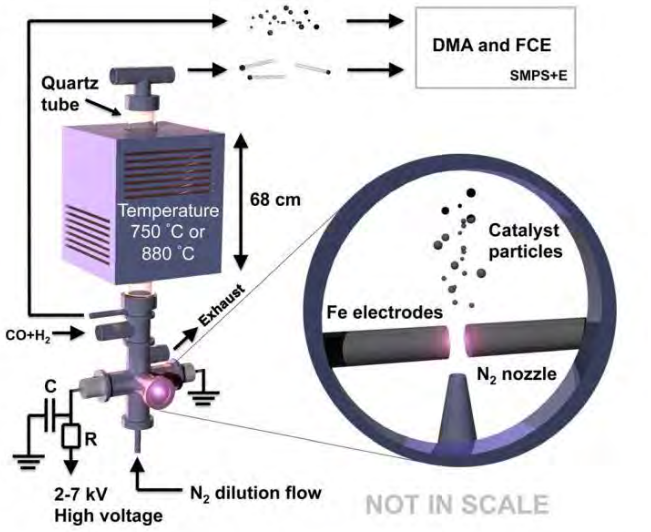

FIG. 1. A schema of the synthesis reactor. The spark generator consists of a pair of iron electrodes separated by a discharge gap, continuously flushed by a high-velocity N_2 jet. The discharges evaporate metal from the electrodes, forming catalyst particles that are subsequently fed into the vertical CVD reactor consisting of a quartz tube in a high temperature furnace. A SMPS + E (scanning mobility particle sizer with electrometer) aerosol size classifier consisting of a differential mobility analyser (DMA) and Faraday cup electrometer (FCE) is used to determine the catalyst number concentrations (N) and geometric mean diameter (D_g) prior to introduction into the reactor, and those of the SWCNTs at the reactor outlet.

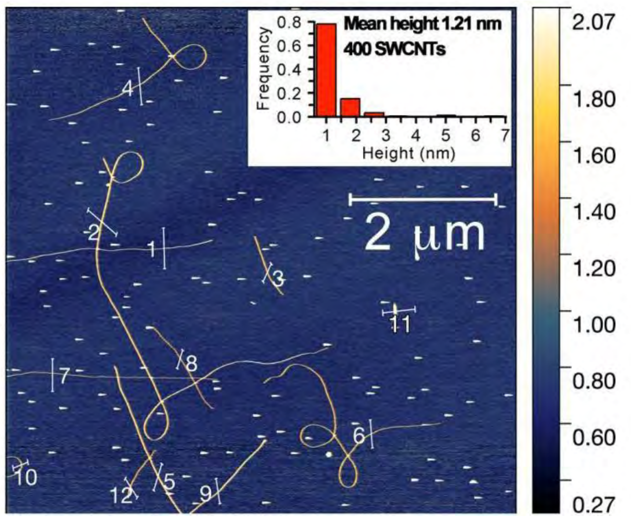

FIG. 4. AFM characterization of SWCNTs synthesized at 880 °C with N ≈ 10^5 cm^{-3}. The scan window size is 7×7 μm^2. The vertical height profiles of the cross sections 1–6 are shown around the scan window, representing heights between 1 and 1.3 nm (profiles 7–12 can be found in Ref. 14). The histogram shows the statistics of 400 height profiles, with the mean at 1.21 nm.

K. Mustonen, P. Laiho, A. Kaskela, Z. Zhu, O. Reynaud, N. Houbenov, Y. Tian, T. Susi, H. Jiang, A. G. Nasibulin, and E. I. Kauppinen. Gas phase synthesis of non-bundled, small diameter single-walled carbon nanotubes with near-armchair chiralities. *Applied Physics Letters*, 107(1):013106, 2015.

vsparticle
Dylec 東京ダイレック株式会社

Developments

Cluster production at atmospheric pressure

2015

- Measurement of Ag clusters in He gas
- Using generic and purified helium gas
- Selection by DMA
- Detection by uCPC

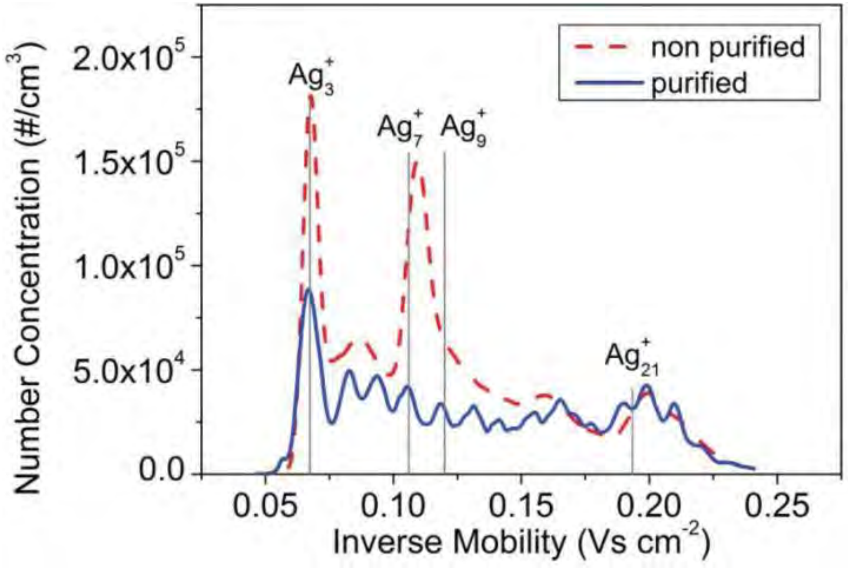

A. Maisser, K. Barmpounis, M. B. Attoui, G. Biskos, and A. Schmidt-Ott. Atomic cluster generation with an atmospheric pressure spark discharge generator. *Aerosol Science and Technology*, 49(10):886–894, 2015.

Developments

Increased yield of charged particles

2016

- A bias voltage is maintained
- This repels positive particles
- The yield is doubled

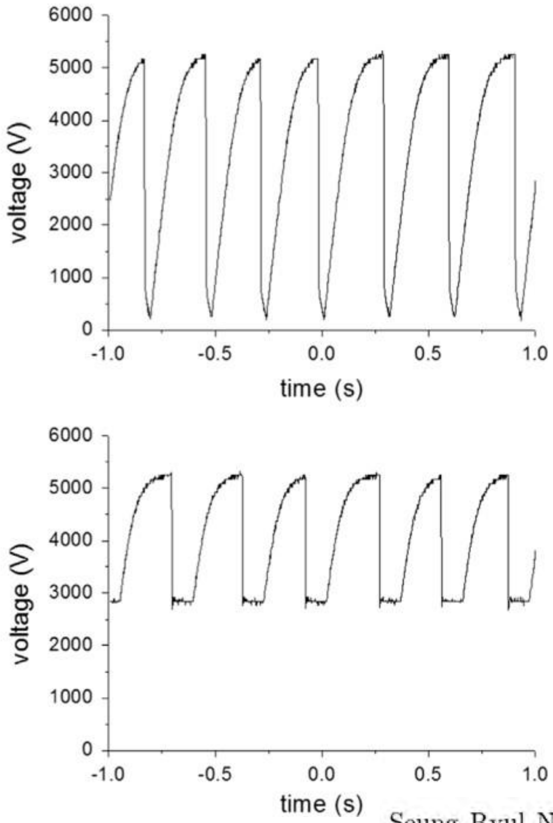

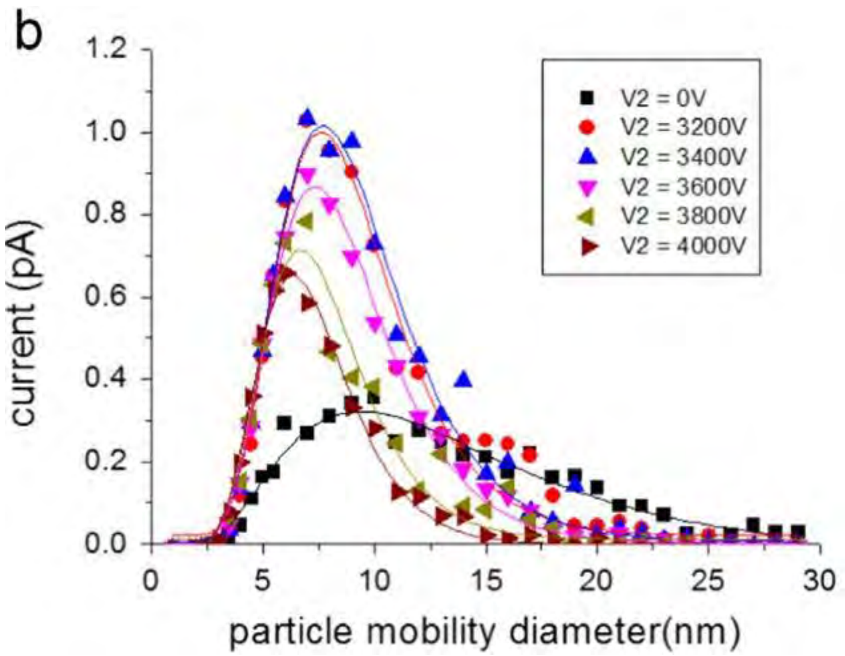

Seung Ryul Noh, Dae Seong Kim, Sei Jin Park, and Mansoo Choi. Enhanced yield of positively charged particles from a spark discharge generator via in situ corona discharges. *Journal of Aerosol Science*, 101:188 – 195, 2016.

vsparticle
Dylec 東京ダイレック株式会社

Developments

Deposition of alloy NPs

2016

- Using alloys as starting materials gives alloyed NPs
- The composition is not affected
- The yield can be predicted

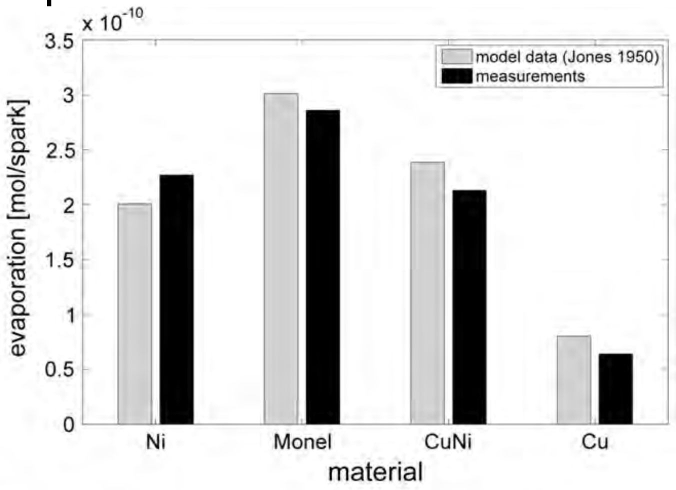

Fig. 5 Comparison of the evaporation rate per spark between the Llewellyn Jones model and the measured data

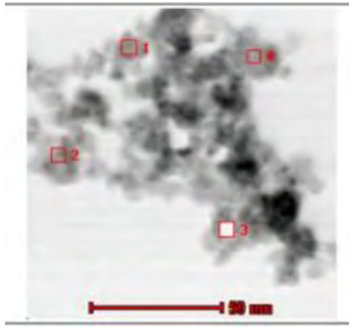

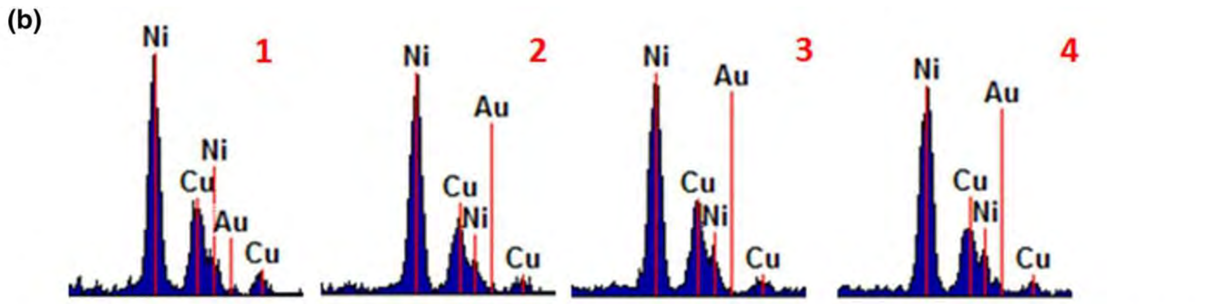

Fig. 8 **a** EDX spectra with the corresponding TEM image using a feedstock with a copper–nickel ration of 40:60, **b** magnification of the spectra for a better visibility

Alex Muntean, Moritz Wagner, Jörg Meyer, and Martin Seipenbusch. Generation of copper, nickel, and cuni alloy nanoparticles by spark discharge. *Journal of Nanoparticle Research*, 18(8):229, Aug 2016.

vsparticle

Dylec

Developments

Temperature and quenching rate of the plasma

2017

- Flow rate of 1.68 slpm
- Plasma temperature around 12000 K
- Quenching rate is around 6×10^8 K/s
- After 25 μs the plasma is at room temperature

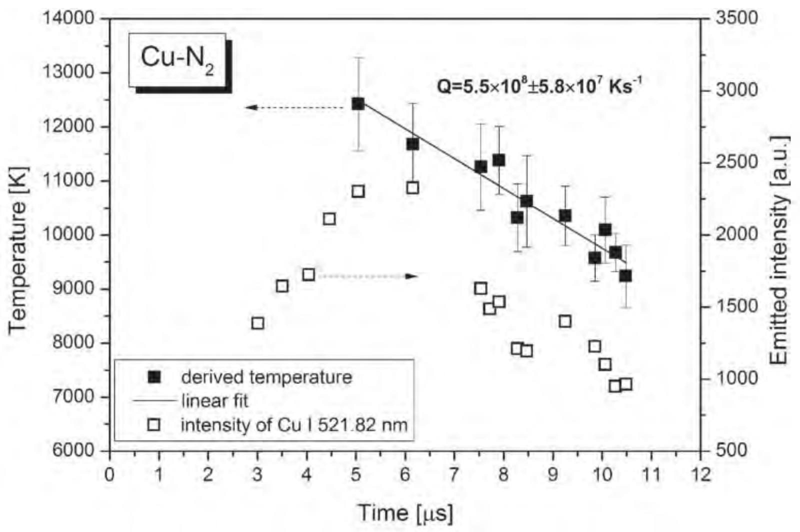

Figure 4. The temporal evolution of the intensity of the Cu I 521.82 nm line (open squares) and the evolution of the temperature of the spark plasma derived from the emission spectra (full squares) (2 mm gap, 1.68 slm gas flow rate, 15 mA charging current).

A Kohut, L Ludvigsson, B O Meuller, K Deppert, M E Messing, G Galbács, and Zs Geretovszky. From plasma to nanoparticles: optical and particle emission of a spark discharge generator. *Nanotechnology*, 28(47):475603, oct 2017.

Developments

Nanopatterning

2017

- Ion-assisted aerosol litography
- Resist is in a + shape
- Deposition of Cu NPs

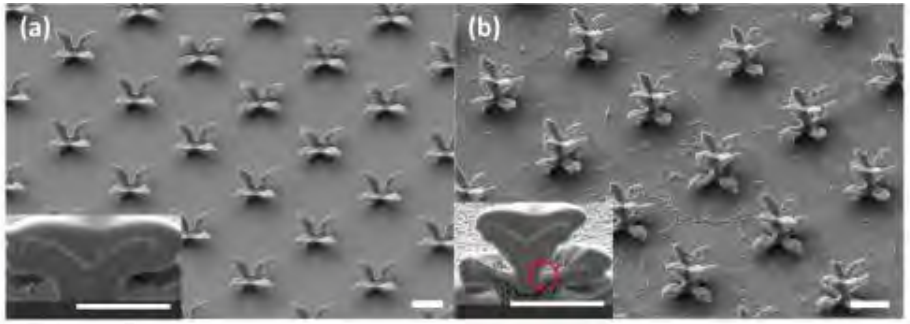

Figure 2. SEM images of (a) mono-layer 3D nanostructures and (b) bi-layer 3D nanostructures. The scale bar represents 1 μm in length.

Kiwoong Lee, Hoseop Choi, Dae Seong Kim, Min Seok Jang, and Mansoo Choi. Vertical stacking of three-dimensional nanostructures via an aerosol lithography for advanced optical applications. *Nanotechnology*, 28(47):475302, oct 2017.

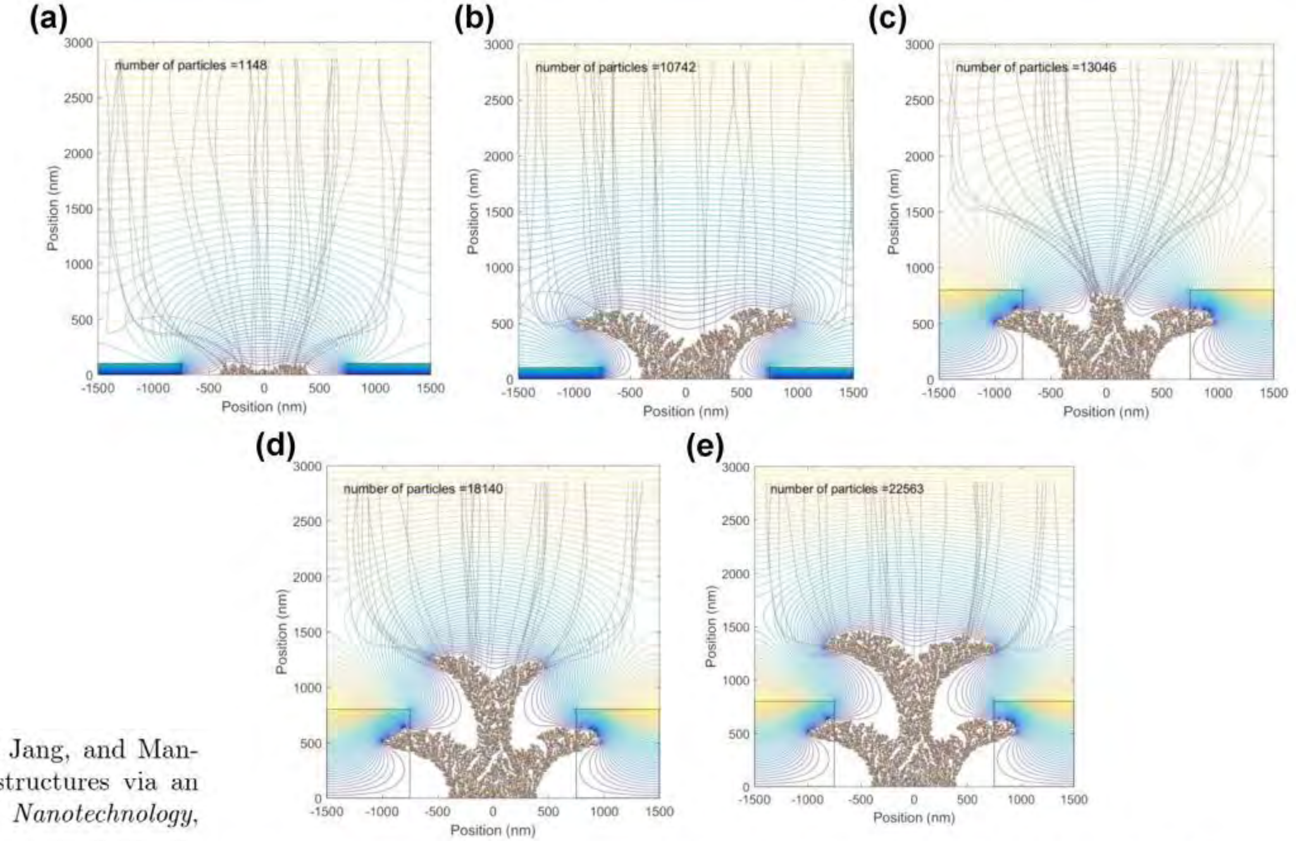

Figure 3. Numerical calculation results for the particle trajectories and deposition under electric potential distributions formed by accumulated charges on the e-beam resist and assembled nanoparticles. (a) Initial growth stage. (b) Formation of mono-layer 3D nanostructure. (c) Initial growth stage of upper 3D nanostructure after additional e-beam lithography. (d), (e) Lateral growth of upper 3D nanostructure.

Developments

Enhanced photocatalysis by plasmonic nanoparticles

2017

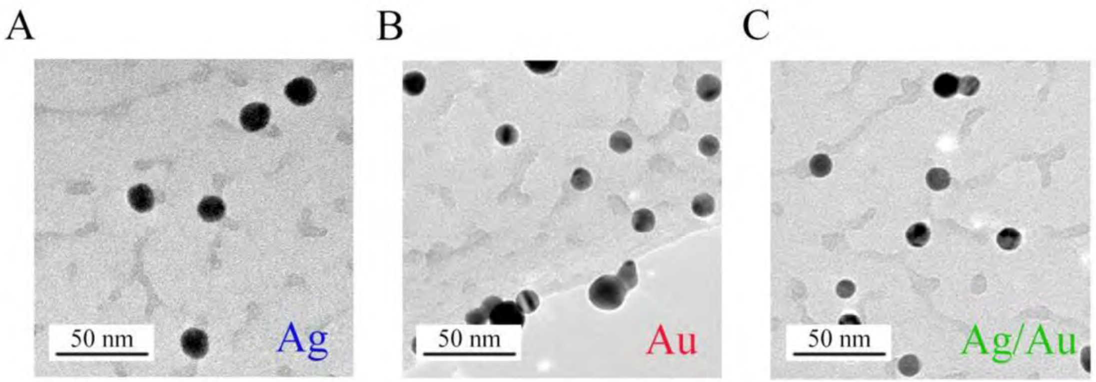

Figure 2. TEM micrographs of the synthesized Ag (A), Au (B) and alloy (C) PNPs.

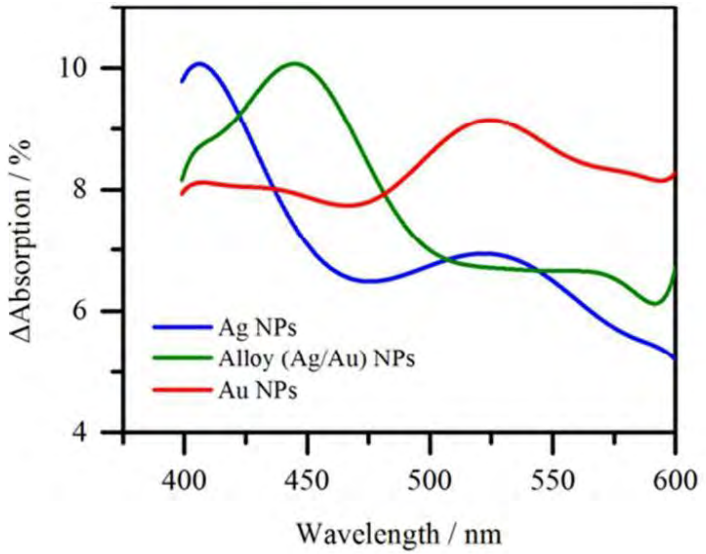

- Deposition of Ag, Au, Ag/Au on TiO_2

Figure 5. A) IPCE enhancement of TiO_2 films when decorated with 15 nm Ag, Alloy (Ag/Au) and Au PNPs at 0.2 V vs. SHE. B) Corresponding absorption increase.

Marco Valenti, Anirudh Venugopal, Daniel Tordera, Magnus P. Jonsson, George Biskos, Andreas Schmidt-Ott, and Wilson A. Smith. Hot carrier generation and extraction of plasmonic alloy nanoparticles. *ACS Photonics*, 4(5):1146–1152, 2017.

Developments

Scale-up by parallelization

2017

- Example of arc-discharge unit
- Production rate scales linearly

Matthias Stein and Frank Einar Kruis. Scaling-up metal nanoparticle production by transferred arc discharge. *Advanced Powder Technology*, 29(12):3138 – 3144, 2018.

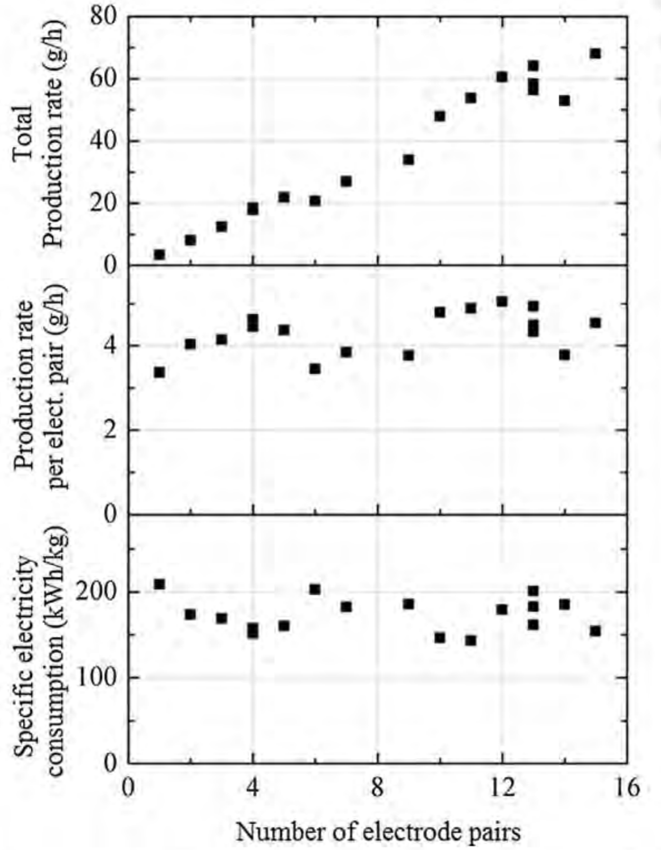

Fig. 7. Production rate (PR_{total}), production rate per electrode pair ($PR_{electrode\ pair}$) and specific electricity consumption (SEC) for copper nanoparticle arc synthesis with different numbers of electrode pairs.

vsparticle

Dylec 東京ダイレック株式会社

Developments

Influence of electrode diameter

2018

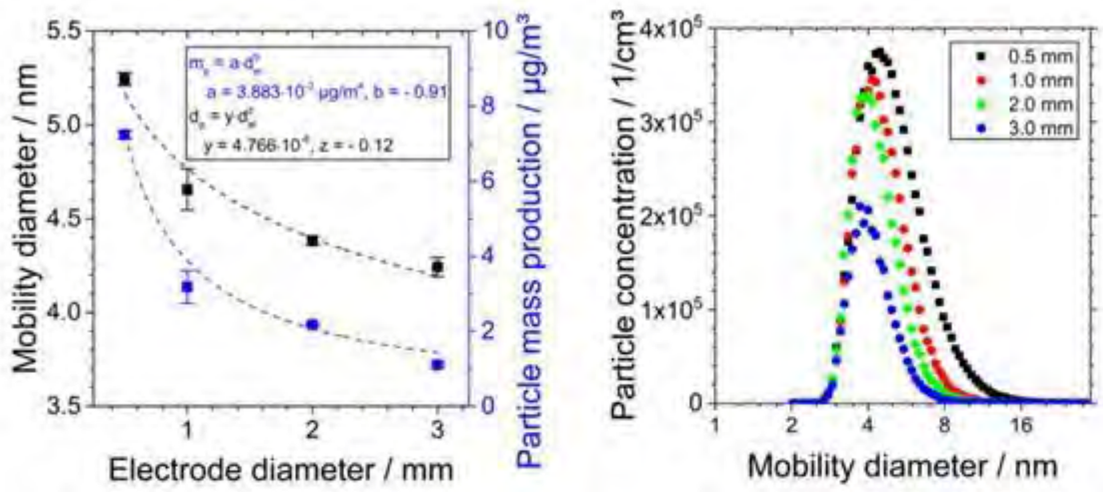

Fig. 8. Influence of copper electrode diameter on particle size and produced mass at standard conditions (left), influence of circuit current on particle size for different copper electrode diameters (middle) and the respective particle size distributions for standard conditions (right).

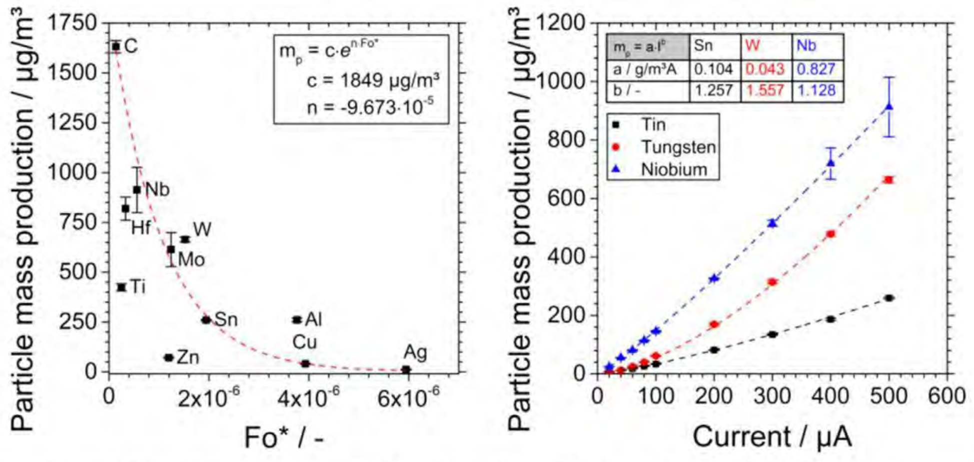

Fig. 9. Dependency of produced particle mass on the modified Fourier number at 500 µA circuit current (left) and on circuit current for the example of tin, tungsten and niobium (right) at otherwise standard conditions.

Maximilian Domaschke, Melanie Schmidt, and Wolfgang Peukert. A model for the particle mass yield in the aerosol synthesis of ultrafine monometallic nanoparticles by spark ablation. *Journal of Aerosol Science*, 126:133 – 142, 2018.

vsparticle

Dylec 東京ダイレック株式会社

Developments

Core-shell particles

2018

- Carbon encapsulation depends on condensation temperature of C:
  - Tm < Tc: core-shell particle
  - Tm ~ Tc: partially filled particle
  - Tm > Tc: composite

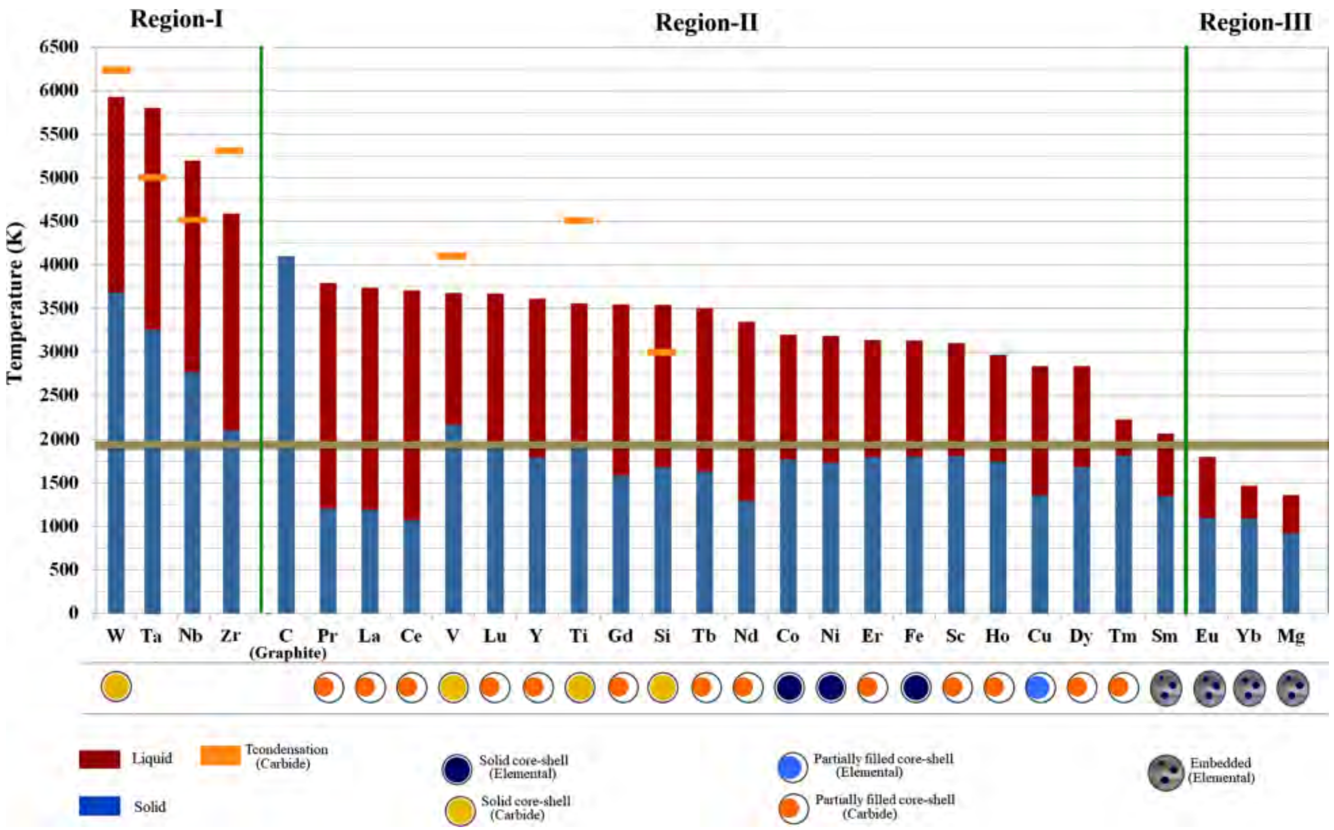

Pelin Livan and Tayfur Ozturk. Carbon encapsulation of elemental nanoparticles by spark discharge. *Journal of Materials Science*, 53(20):14350–14360, Oct 2018.

vsparticle
Dylec 東京ダイレック株式会社

Developments

Production of SERS samples

2018

- Silver nanoparticles

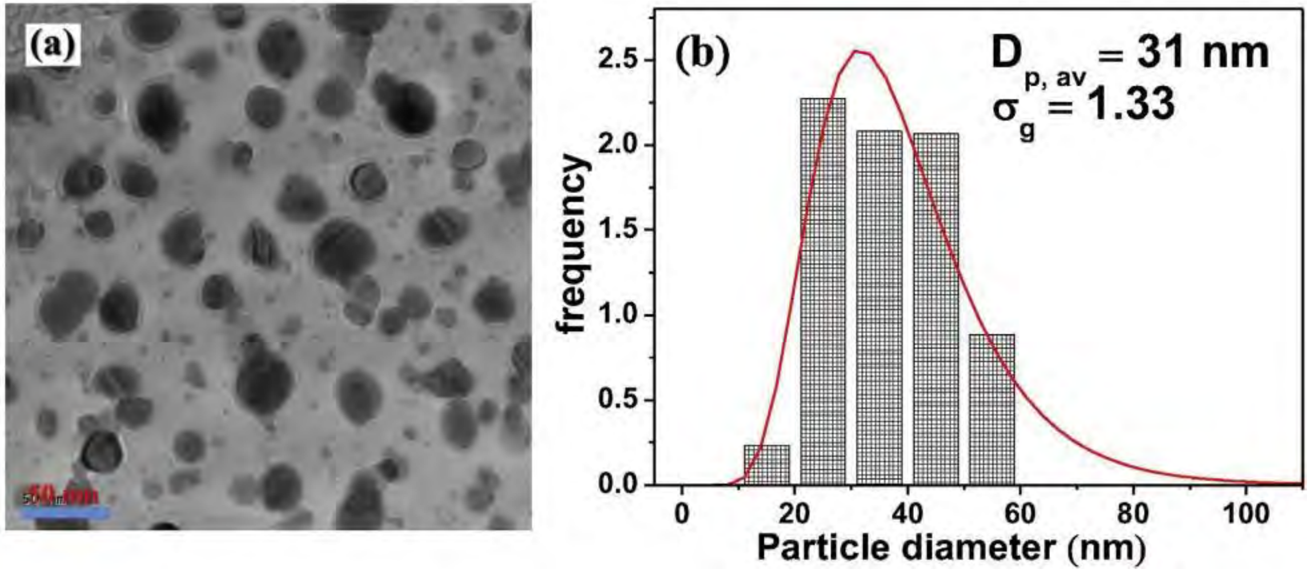

Mohamed Abd El-Aal, Takafumi Seto, Mikio Kumita, Ayman A. Abdelaziz, and Yoshio Otani. Synthesis of silver nanoparticles film by spark discharge deposition for surface-enhanced raman scattering. *Optical Materials*, 83:263 – 271, 2018.

vsparticle

Dylec 東京ダイレック株式会社

Developments

Making alloyed NPs using elemental electrodes

2018

- Ablation produces ions and electrons
- Ions have a stronger albation compared to electrons
- Discharge is oscillatory

  and can be manipulated

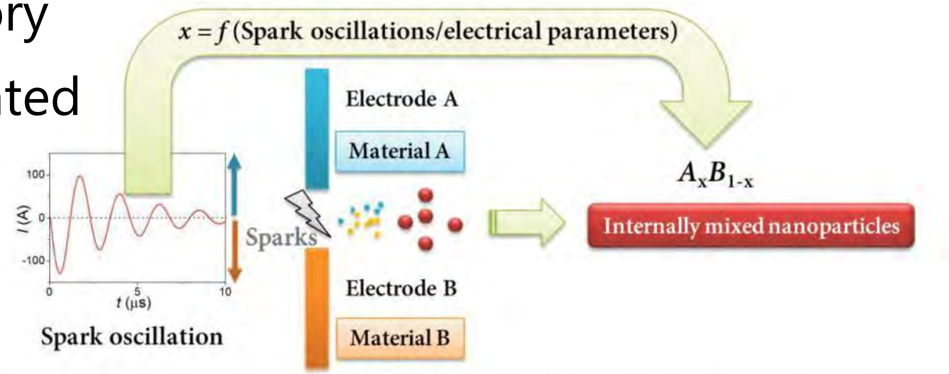

Figure 1. Schematic illustration of internal NP mixing by using two different electrodes. Variable x indicates the fraction of one (here is material A) electrode material in the resulting NPs, which in turn have a composition distribution. Spatial distribution of vapors produced by the two different electrodes can lead to NPs composed of a single element (i.e., $x = 0$ or 1).

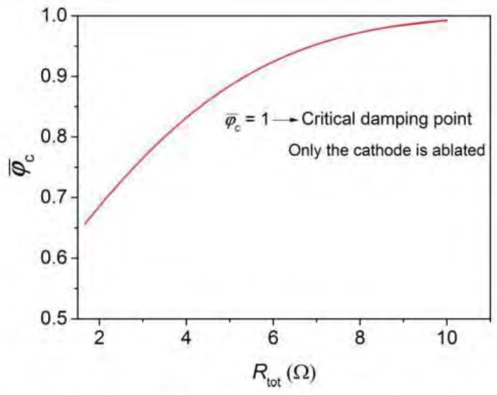

Figure 5. Mean mixing ratio $\overline{\varphi}_C$ as a function of the total resistance R_{tot} used in the spark circuit for $C_A = C_C$ ($C_{ca} = 45$ nF, $L_i = 3$ μH). When R_{tot} increases to a critical damping point ($R_{tot}^2 = 4L_i/C_{ca}$, $R_{tot} \approx 16$ Ω), only the cathode is ablated due to no polarity reversal.

Jicheng Feng, Nabil Ramlawi, George Biskos, and Andreas Schmidt-Ott. Internally mixed nanoparticles from oscillatory spark ablation between electrodes of different materials. *Aerosol Science and Technology*, 52(5):505–514, 2018.

vsparticle
Dylec 東京ダイレック株式会社

Developments

Preventing oxidation

2018

- Hydrogen is a reducing agent

Table 2. Composition and identified phases of compacted nanoparticles generated in a hydrogen mixture or in nitrogen.

			Oxygen (XEDS)		Crystal structure	
H_2 (%)	Electrode material	Sinter temperature (°C)	(at%)	(wt%)	XRD	TEM
5	Bismuth	400	34 ± 13	04 ± 1	Bi	Bi
5	Tin	900	34 ± 11	07 ± 3	Sn	Sn
5	Cobalt	700	40 ± 16	15 ± 9	Co	Co
5	Gold	500	27 ± 20	03 ± 2	—	Au
0	Bismuth	500	60 ± 07	10 ± 3	Bi and Bi_3O_4	Bi and Bi_3O_4
0	Tin	900	72 ± 07	26 ± 7	Low signal*	Sn and/or SnO and SnO_2
0	Cobalt	700	61 ± 05	30 ± 4	Low signal*	CoO
0	Gold	500	25 ± 10	03 ± 1	—	Au

*The particle concentration was too low for XRD.

R. T. Hallberg, L. Ludvigsson, C. Preger, B. O. Meuller, K. A. Dick and M. E. Messing. Hydrogen-assisted spark discharge generated meta nanoparticles to prevent oxide formation. *Aerosol Science and Technology* 52(3):347–358, 2018.

Developments

Self aligning growth of NP-based interconnects

2018

- text

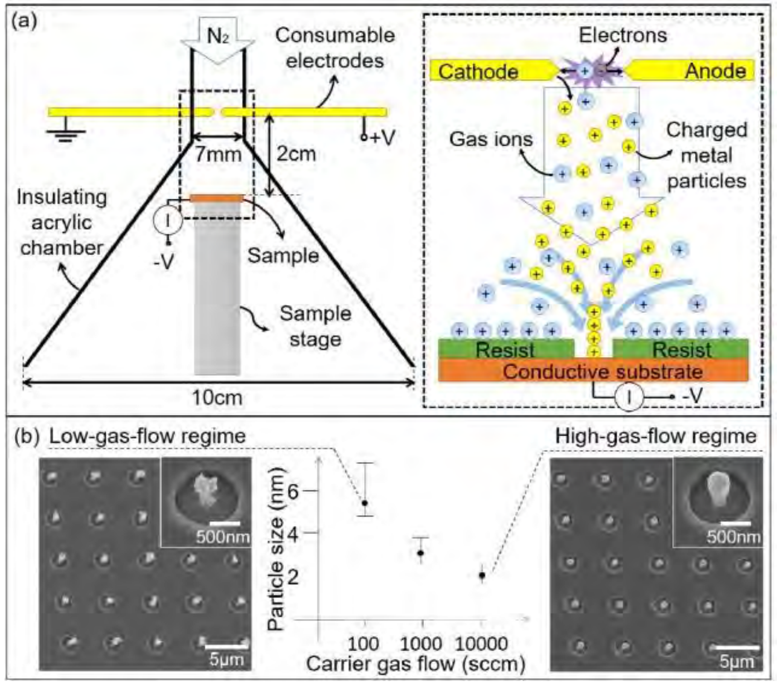

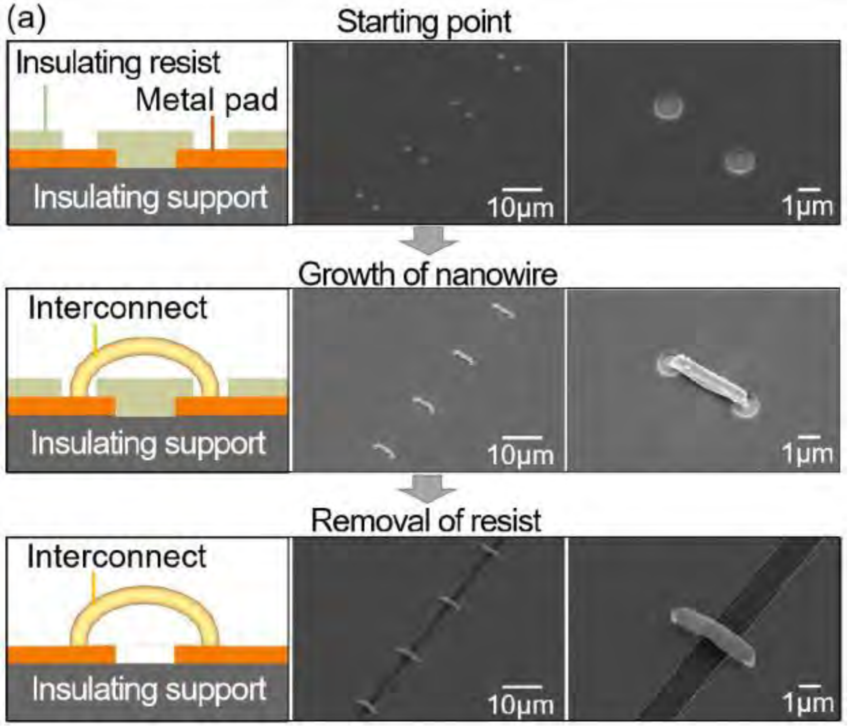

S. Leslie, I. Nishchay, N. Helene, R. Johannes Thomas, P. Jörg, and J. Heiko. Self aligning growth of nanoparticle-based interconnects. In *2018 IEEE 13th Nanotechnology Materials and Devices Conference (NMDC)*, pages 1–4, Oct 2018.

Developments

Electrochemical sensor

2019

- text

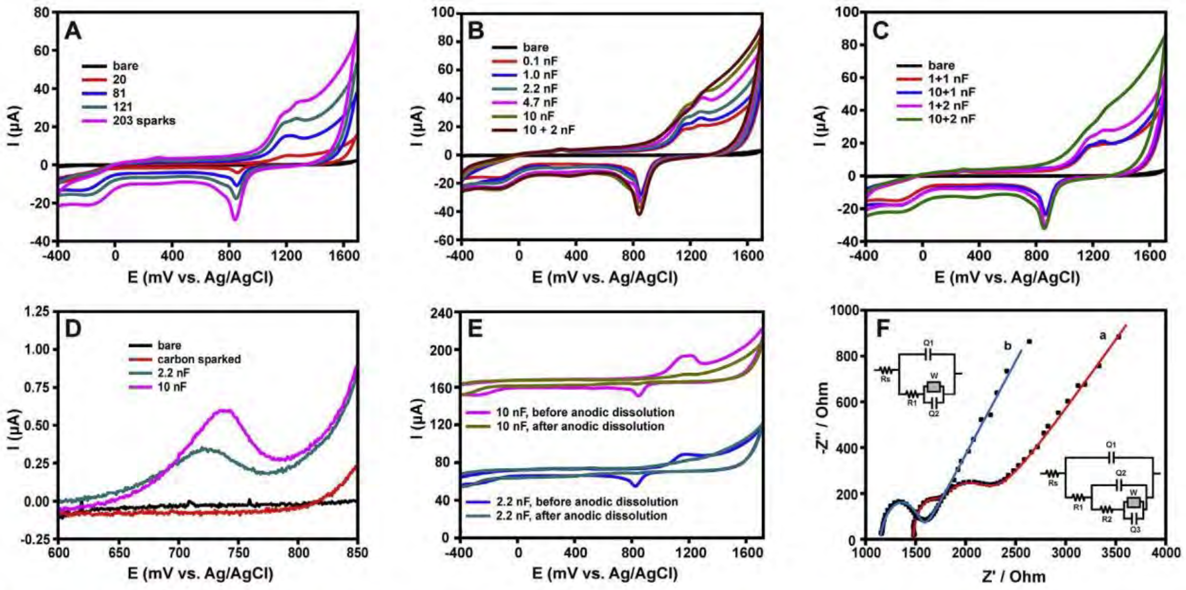

Fig. 5. CVs of gold redox transitions in 0.1 M H_2SO_4 in dependence on the number of sparks (A) and the values of capacitors in the Cockroft-Walton cascade (C_{int}) and external capacitors (B,C). Anodic dissolution of gold during LSV in 10 mM KBr and 0.1 M $HClO_4$ at 5 mV/s (D). CVs in 0.1 M H_2SO_4 before and after anodic dissolution experiment (E, CVs have been offset along the y-axis for clarity). The CVs in H_2SO_4 were measured at 100 mV/s; V_{spark} = 1.2 kV; spark cycles: 203 (B), 121 (C); C_{int} = 2.2 nF (A). Nyquist plots of eAu/Si-SPEs (F) modified with 43 (scan a) and 203 (scan b) sparking cycles at V_{spark} = 1.2 kV, C_{int} = 10 nF. (For interpretation of the references to colour in this figure legend, the reader is referred to the Web version of this article.)

Maria G. Trachioti, Eleni I. Tzianni, Daniel Riman, Jana Jurmanova, Mamas I. Prodromidis, and Jan Hrbac. Extended coverage of screen-printed graphite electrodes by spark discharge produced gold nanoparticles with a 3d positioning device. assessment of sparking voltage-time characteristics to develop sensors with advanced electrocatalytic properties. *Electrochimica Acta*, 304:292 – 300, 2019.

vsparticle

Dylec 東京ダイレック株式会社

お問合せ先

Email: info@tokyo-dylec.co.jp

Tel: 03-5367-0891（営業部）

Dylec 東京ダイレック株式会社
TOKYO DYLEC CORP.

vsparticle